Biomacromolecules

Open Access

This article is licensed under CC-BY-NC-ND 4.0

pubs.acs.org/Biomac

Article

Permselectivity of Silk Fibroin Hydrogels for Advanced Drug Delivery Neurotherapies

Rocío Fernández-Serra, Amira Lekouaghet, Lorena Peracho, Mahdi Yonesi, Alberto Alcázar, Mourad Chioua, José Marco-Contelles, José Pérez-Rigueiro, Francisco J. Rojo, Fivos Panetsos, Gustavo V. Guinea, and Daniel González-Nieto*

Cite This: *Biomacromolecules* 2024, 25, 5233−5250

Read Online

ACCESS | Metrics & More | Article Recommendations | Supporting Information

ABSTRACT: A promising trend in tissue engineering is using biomaterials to improve the control of drug concentration in targeted tissue. These vehicular systems are of specific interest when the required treatment time window is higher than the stability of therapeutic molecules in the body. Herein, the capacity of silk fibroin hydrogels to release different molecules and drugs in a sustained manner was evaluated. We found that a biomaterial format, obtained by an entirely aqueous-based process, could release molecules of variable molecular weight and charge with a preferential delivery of negatively charged molecules. Although the theoretical modeling suggested that drug delivery was more likely to be driven by Fickian diffusion, the external media had a considerable influence on the release, with lipophilic organic solvents such as acetonitrile−methanol (ACN−MeOH) intensifying the release of hydrophobic molecules. Second, we found that silk fibroin could be used as a vehicular system to treat a variety of brain disorders as this biomaterial sustained the release of different factors with neurotrophic (brain-derived neurotrophic factor) (BDNF), chemoattractant (C-X-C motif chemokine 12) (CXCL12), anti-inflammatory (TGF-β-1), and angiogenic (VEGF) capacities. Finally, we demonstrated that this biomaterial hydrogel could release cholesteronitrone ISQ201, a nitrone with antioxidant capacity, showing neuroprotective activity in an in vitro model of ischemia-reoxygenation. Given the slow degradation rate shown by silk fibroin in many biological tissues, including the nervous system, our study expands the restricted list of drug delivery-based biomaterial systems with therapeutic capacity for both short- and especially long-term treatment windows and has merit for use with brain pathologies.

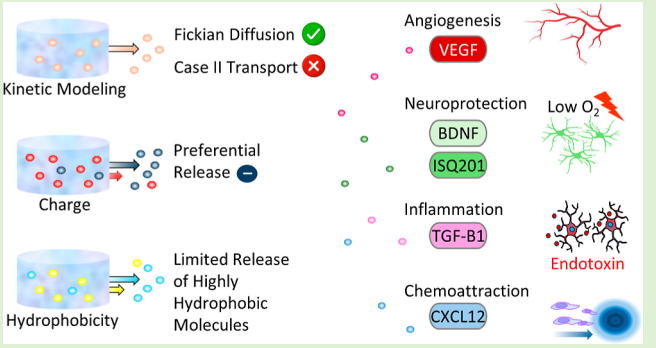

1. INTRODUCTION

Intensive preclinical research has been performed in recent decades to develop biomaterial-based drug delivery systems to treat a wide range of pathologies.[1] These systems mainly aim to increase the drug stability and overcome physiological barriers that hamper drug mobilization to the target tissue. In addition, biomaterials have been designed to achieve better temporal control of drug concentrations within therapeutic ranges. This is especially relevant when adjusting the duration of treatment for the time required either to modify the pathological signals that exacerbate the injury or to stop the progression of damage. Several of these systems have been developed to attenuate the inflammatory response or oxidative stress[2] or to remove or sequester abnormal molecules or misfolded proteins.[3] Drug delivery applications are especially relevant in particular conditions that require prolonged treatments; for instance, biomaterials may stimulate endogenous repair mechanisms either by replacing damaged tissues and/or remodeling intact areas toward tissue respecialization to restore physiological functions that were lost after the injury.

Currently, a number of clinical applications support the use of biomaterials for the pharmacological release of molecules in tissues.[4] However, and probably because of their complexity, the clinical use of biomaterials for drug delivery in the nervous system is much more marginal, with only a few exceptions such as the implantable carmustine wafer commercially known as Gliadel that is being used to treat malignant glioma.[5] However, several preclinical studies highlight the advantages of using biomaterials to target the central nervous system (CNS),[6] especially to overcome the hermeticism of the blood−brain barrier (BBB) and the clearance capacity of the brain for rapid removal of drugs and diverse molecules from the tissue parenchyma. The BBB and this clearance capacity probably

Received: May 9, 2024
Revised: May 20, 2024
Accepted: May 21, 2024
Published: July 17, 2024

Downloaded via UNIV COMPLUTENSE DE MADRID on February 13, 2025 at 12:46:28 (UTC).
See https://pubs.acs.org/sharingguidelines for options on how to legitimately share published articles.

© 2024 The Authors. Published by American Chemical Society

https://doi.org/10.1021/acs.biomac.4c00629
Biomacromolecules 2024, 25, 5233−5250

constitute the main bottlenecks in the classical administration routes of drugs to the CNS.

Different mechanisms may influence the delivery of molecules from distinct biomaterials. However, a general model of drug release that encompasses all biomaterials and formats tested has not yet been established. For example, the delivery of different chemoattractant molecules such as CXCL12 or CXCL10 from alginate hydrogel microspheres is largely determined by electrostatic interactions with the alginate matrix.[7] In another study, the rate of delivery of angiogenic factors such as VEGF and Ang1 was dependent on the molecular weight of the PLGA microspheres embedded in a hyaluronic acid hydrogel.[8] Even the rate and extent of drug delivery, e.g., from chitosan-based nanoparticles or silk fibroin hydrogels, can be conditioned by the external media.[9] The absence of specific rules that define the release of different molecules from a biomaterial means that these mechanisms must be studied on a case-by-case basis for each biomaterial, composition, and format.

Silk fibroin (SF) is a prominent biomaterial that can be used for pharmacological administration because of two specific properties: poor immunogenicity and high stability with in vivo resistance to degradation even under inflammatory conditions.[10] In the context of the CNS, the limited but theoretically controllable degradability of SF can be exploited where either short[11] or extended[12] drug delivery times are required. Previous studies illustrate a wide range of possibilities of using SF in formats such as nanoparticles, films, fibers, microspheres, and hydrogels[13] to gradually deliver small[14] and large[15] molecules in various tissues. However, most of these studies focused on noncerebral tissues, whereas the use of SF to target the CNS has been less frequent.

Importantly, SF hydrogels are relatively well matched with the mechanical properties of brain tissue and can avoid interference with self-remodeling processes when this format is intracerebrally injected. The possibility of transforming silk proteins in smart materials with shape memory features has also profound repercussions in the neurology field. Injectable silk sericin scaffolds with programmable shape-memory have been used to fit the irregular stroke cavity,[16] and new feasible strategies are being used for the design of shape memory biomaterials, for example, merging 3D printing with cold programming (environmental temperature) to create porous predefined geometries.[17] The hydrogel format is also particularly relevant for delivering drugs to the CNS via the intranasal route. Understanding how hydrogels can release certain molecules and not others on the basis of their chemical nature, including their temporal dynamics of delivery, is key to optimizing future designs. Several in vitro and in vivo studies have been conducted to explore the release of different molecules from different SF-based biomaterial formats. For example, SF hydrogels have been designed to deliver chemoattractant chemokines,[18] antiangiogenic factors,[19] or antitumoral drugs.[20] To understand the permselectivity properties of SF in a hydrogel format, the first part of this study explored the preferential ability of SF hydrogels, which had been entirely fabricated through an aqueous-based procedure, to deliver molecules that vary in size, charge, and hydrophobicity. Then, to evaluate the use of SF hydrogels in strategies that aim to enhance neuroprotection and brain plasticity, the kinetic course and sustained activity of five relevant CNS-related molecules delivered by SF hydrogels were assessed.

Our results demonstrate the versatility of SF hydrogels for the direct release of molecules to target the nervous system, which may pave the way to develop therapeutic strategies to treat acute and chronic brain damage.

2. MATERIALS AND METHODS

2.1. SF Extraction and Preparation of SF Hydrogels. SF extraction was conducted following previous methodologies.[21] *Bombyx mori* silkworm cocoons were generously supplied by Professors José Luis Cenis and Salvador D. Aznar-Cervantes (IMIDA, Murcia, Spain). The cocoons were carefully cut into small pieces of approximately 2 cm^2 and degummed in an autoclave (Tuttnauer 5075 MLV) at 121 °C for 30 min while immersed in a 0.2% (w/v) sodium carbonate solution (Panreac Quimica). After removal of silk sericin, degummed cocoons were thoroughly rinsed with distilled water, dried, and subsequently dissolved in a 9.3 M lithium bromide solution (Thermo Fisher Scientific) for 4 h at 60 °C. The resulting SF solution was dialyzed against distilled water inside 3.5 kDa cutoff dialysis membranes until electroconductivity of the water was below 10 μS/cm. Finally, the lithium bromide-free solution of silk was frozen at −80 °C and lyophilized using a LyoQuest freeze-dryer (Telstar).

To prepare SF hydrogels, 2 and 6% (w/v) SF solutions were formulated in phosphate-buffered saline (PBS) and sonicated using a Branson model 450 sonifier (Branson Ultrasonics Co.) equipped with a 3 mm diameter−tapered microtip. Sonication was performed at 15% amplitude for 15 min while maintaining the solutions at 40 °C throughout the process. Processing parameters were selected in order to induce a delayed gelation process in a time window of 10−30 min.

2.2. Mechanical Characterization of SF Hydrogels. The mechanical characterization of SF hydrogels was conducted using uniaxial unconfined compression tests in air on gels with the same composition as those later used for the release experiments.[21] 24 h after sonication, gels were carefully cut into cylinders (12.5 mm diameter and 10.0 mm height) and positioned between two parallel plates for testing.

The uniaxial compression tests were performed using an Instron 4411 testing machine under a constant displacement rate of 1.8 mm/min. The force applied to the sample was continuously monitored by a Precisa XT220 scale positioned beneath the lower plate. Samples were compressed until failure. Stress−strain curves (σ and ε) were derived from force and displacement data. Stress was calculated as the instantaneous force divided by the initial cross-sectional area. Strain was calculated as the instantaneous displacement divided by the initial height of the specimen. Stress and strain at break (σb and εb) were determined from the point of failure. The initial modulus of elasticity (E_i) for each curve was obtained by the slope of the stress−strain curve at strain range of 1−3%.

2.3. Secondary Structure of SF Hydrogels. The secondary structure of SF hydrogels was determined before and 24 h after sonication. Attenuated total reflectance-Fourier transform infrared (ATR-FTIR) spectroscopy was performed in a Nicolet iS5 FTIR spectrometer with an ATR iD5 complement. A background spectrum was first obtained from PBS. All spectra were the average of 32 scans from 550 to 4000 cm^{-1} with a resolution of 4 cm^{-1}. The contribution of the different secondary structures in SF solutions and hydrogels were obtained after deconvolution of the amide peak I (1580−1720 cm^{-1}) using the software OMNIC 9.0 (Thermo Fisher Scientific Inc.). To achieve this, the amide I peak was selected and fitted to Gaussian functions, following previous methodologies.[22] The areas of the Gaussian functions at fixed wavelengths served to estimate the content of the different secondary structures as follows: intermolecular β-sheets (ascribed to 1615, 1624, and 1700 cm^{-1}), intramolecular β-sheets (1632 cm^{-1}), random coils (1641 cm^{-1}), α-helices (1660 cm^{-1}), and β-turns (1680 cm^{-1}).

2.4. In Vitro Release of Fluorescent Molecules from SF Hydrogels. To explore the ability of SF hydrogels to deliver molecules of different sizes, charges, and hydrophobicities, several formulations of SF with different fluorescent molecules were separately prepared. The ALOGPS application (VCCLAB; https://vcclab.org/) was employed to predict hydrophobicity (Log P). The Log P value, also referred to as the octanol−water partition coefficient, provides a quantitative measurement of a molecule's hydrophobicity and is predicted by

https://doi.org/10.1021/acs.biomac.4c00629
Biomacromolecules 2024, 25, 5233−5250

Table 1. Fluorescent Molecules and Total Mass Encapsulated in SF Hydrogels

molecule	mass (μg)	λ excitation (nm)	λ emission (nm)	supplier
calcein blue (CB)	0.24	322	445	Sigma-Aldrich (M1255)
carboxyfluorescein (CF)	0.28	492	517	Invitrogen (C194)
propidium iodide (PI)	0.50	482	608	Sigma-Aldrich (P4170)
FITC-dextran	20	494	518	Invitrogen (D1820)

Table 2. Proteins Factors and Total Mass Encapsulated in SF Hydrogels

molecule	mass (kinetics assays) (ng)	mass (functional assays) (ng)	protein factors (suppliers)	ELISA (R&D systems)
BDNF	2	14	Peprotech (450−02)	DBNT00
VEGF	2	14	Peprotech (450−32)	MMV00
CXCL12	10	40	Peprotech (250−20A)	MCX120
TGF-β-1	1.7	12	R&D Systems (7666 MB)	DB100C

analyzing its structure. A 70 μL volume of 2 or 6% SF hydrogels in the pregel state was separately mixed with the specific quantity of each molecule indicated in Table 1.

These hydrogel formulations were then dispensed into individual wells of a 96-well plate and allowed to gel at 37 °C. Following complete gelation, 100 μL of PBS was added per well and the released medium was collected at different time points (10 min; 1, 2, 3, 4, and 24 h; and 3 and 7 d). Fluorescence images were captured for the collected media (to assess released molecules) by using a Leica DMI3000B fluorescence microscope connected to a DFC340-FX monochrome digital camera and tuned to the corresponding excitation and emission wavelengths of each molecule (Table 1). A pseudocolor was applied to the images based on the emission of each molecule. Fluorescence intensity measurements were conducted using ImageJ based on mean pixel intensity. To avoid a possible interference of SF autofluorescence, for each experiment, three replicates of 70 μL blank hydrogels (with no fluorescent molecules inside) were used. Fluorescence images of the collected media from these blank hydrogels were taken with the same parameters as for each of the fluorescent molecules. The average fluorescence intensity present in the release media of blank hydrogels was subtracted from the fluorescence intensity detected in the release media from each fluorescence molecule. Fluorescence images were also taken of the hydrogels to assess the amount of retained fluorescent molecules.

2.5. Release Kinetics from SF Hydrogels. To fit the release kinetics of the fluorescent molecules from the biomaterial, the percentage of cumulative delivery versus time was fitted to three phenomenological models as follows

i Korsmeyer−Peppas[23] $\frac{M_t}{M_\infty} = k \cdot t^n$

ii Peppas−Sahlin[24] $\frac{M_t}{M_\infty} = k_1 \cdot t^m + k_2 \cdot t^{2m}$

iii Weibull[25] $\frac{M_t}{M_\infty} = 1 - e^{-\alpha t \beta}$

In all of the equations, M_t/M_∞ represents the fraction of drug released at time t. In the Korsmeyer−Peppas equation, k is a constant dependent on the characteristics of the polymer and the drug and n is the diffusional exponent that is independent of the geometry of the sample. In the Peppas−Sahlin equation, $k_1 \cdot t^m + k_2 \cdot t^{2m}$, Fickian diffusion and a polymer relaxation contribution are considered corresponding to each term. The Weibull equation is useful for comparing the delivery time course between different molecules, although this equation does not provide specific information on release mechanisms. In the Weibull model, α is a parameter that defines the time scale of the process, and β characterizes the curve shape (exponential, sigmoid, or parabolic). The percentages of cumulative release across the time were fitted to each model using the DDSolver add-in included in Microsoft Office Excel. The first 60% of all release curves was used for statistical analysis. The goodness of fitting was based on a higher coefficient of determination (R^2) and a lower Akaike information criterion (AIC) (parameters also provided by the DDSolver add-in program).

2.6. Release of Neurovascular and Anti-Inflammatory Factors from SF Hydrogels. The release of four different proteins was studied: brain-derived neurotrophic factor (BDNF), vascular endothelial growth factor (VEGF), stromal cell-derived factor 1 (SDF-1, also known as CXCL12), and transforming growth factor β1 (TGF-β-1). For the release kinetic studies, different amounts of these molecules were noncovalently incorporated into SF solutions (kinetics assays in Table 2) immediately after sonication. After gelation, the hydrogels were incubated with 100 μL of 0.1% (w/v) bovine serum albumin (BSA) in PBS. The delivery medium was collected at various time points (10 min, 2 h, and 1, 3, and 7 d) and stored at −20 °C for subsequent analysis. The protein concentration in the delivery medium was quantified using enzyme-linked immunosorbent assays (ELISAs) following the manufacturer's instructions (R&D Systems).

To assess the sustained functionality of the delivered molecules, the four proteins were reconstituted with SF solutions (functional assays in Table 2). Following gelation, the hydrogels were incubated with 100 μL of Dulbecco's modified Eagle medium (DMEM) containing 0.1% (w/v) BSA. Delivery media were collected at different time intervals after gelation (0−1 and 3−7 days), and the samples were frozen at −20 °C.

2.7. Release of the Nitrone ISQ201 from SF Hydrogels. To examine the capacity of SF hydrogels to deliver the cholesteronitrone ChNF2 (ISQ201),[26] several formulations of SF with ISQ201 were separately prepared. The preparation of these formulations was conducted following procedures similar to those described above, and 10 mg of ISQ201 was incorporated in 70 μL of 2 and 6% SF hydrogels. After the gelation process was complete, hydrogels were incubated with 100 μL of PBS. The release of ISQ201 from the hydrogels was analyzed 2, 24, and 72 h after drug encapsulation. Media collected at these time points were frozen until further analysis by mass spectrometry.

2.8. Detection and Quantification of Nitrone ISQ201 by Mass Spectrometry. The quantification of ISQ201 present in the released media was performed with 20 μL of each elution medium mixed with 1 μL of olesoxime (0.21 mM), which was added as an internal standard (IS). The resulting solution was mixed 1:1 (v/v) with 2,5-dihydroxybenzoic acid matrix (Bruker-Daltonics) at 10 mg/mL in acetonitrile/methanol (ACN−MeOH) (50:50, v/v). Subsequently, 0.5 μL of the mixture was spotted onto a ground steel target plate (Bruker-Daltonics), dried, and assessed via matrix-assisted laser desorption/ionization time-of-flight (MALDI-TOF) mass spectrometry analysis (Autoflex III, Bruker-Daltonics). Compound ISQ201 (413.36 Da) was detected through its primary peak at m/z 398.378 ([M + H]+), corresponding to the loss of an oxygen atom attached to nitrogen. Similarly, the IS (399.35 Da) was detected through its peak at m/z 384.362 ([M + H]+), representing the molecule resulting from the loss of a hydroxyl group. The quantification of ISQ201 in each sample was performed measuring the peak intensity of ISQ201 and the IS in the same spectra as a ratio of ISQ201/IS. Ratios were then interpolated into a calibration curve for ISQ201 (range 1−100 μM) to calculate the ISQ201 concentration in the released media.

2.9. Biological Assessments. *2.9.1. Brain-Derived Neurotrophic Factor.* The sustained functionality of BDNF released from SF hydrogels was inferred from the analysis of survival and differentiation of Neuro 2A (N2A) cells.[27] N2A cells, kindly donated by Dr. Luis

https://doi.org/10.1021/acs.biomac.4c00629
Biomacromolecules 2024, 25, 5233−5250

Barrio (Hospital Universitario Ramón y Cajal), were cultured in complete medium comprising DMEM supplemented with 10% (v/v) inactivated fetal bovine serum (FBS), 1% (v/v) penicillin/streptomycin (P/S), and 2 mM l-glutamine (L-Gln). To evaluate the biological activity of BDNF, N2A cells were seeded in 24-well plates at 5×10^3 cells per well. After 4 days of incubation, the complete medium was replaced with FBS-free medium, and wells were divided into different groups: −BDNF, +BDNF at concentrations of 5, 10, and 20 ng/mL, or delivery medium collected from BDNF-SF hydrogels of 2 and 6% concentrations and two different release time periods (0−1 and 3−7 d). The release medium was supplemented with 1% P/S and 2 mM l-Gln. After 3 days of incubation in conditioned medium, cells were stained with calcein-acetoxymethyl ester (calcein-AM; Invitrogen), and fluorescence images were captured using a fluorescence microscope (Leica DMI3000B). Image analysis was performed using ImageJ (NIH). Cell survival was determined by counting the number of cells in each well, whereas differentiation was calculated based on the number of cells with processes relative to the total cells in the image field, following a methodology previously described.[28]

2.9.2. Vascular Endothelial Growth Factor. The sustained functionality of VEGF released from SF hydrogels was evaluated by assessing the differentiation of hemangioendothelioma cells (EOMAs) into capillary-like tubular structures. EOMA cells, generously provided by Dr. Luisa María Botella (Centro de Investigaciones Biológicas, CSIC), were cultured in complete medium on gelatin-coated plates prepared in 0.2% (w/v) PBS. The tubular structure formation assay was conducted following the protocol developed by DeCicco-Skinner and colleagues.[29] 24 h before the experiment, the complete medium was replaced with fasting medium (DMEM, 0.2% FBS, 1% P/S, and 2 mM L-Gln). The assay was performed in 96-well plates coated with 70 μL of Matrigel with a reduced growth factor content (Corning 356230). EOMA cells were seeded on the Matrigel matrix at 15×10^3 cells per well.

Wells were divided into different groups: −VEGF, +VEGF at 5, 10, and 20 ng/mL, or delivery media collected from VEGF-SF hydrogels of 2 and 6% with two different release time periods (0−1 and 3−7 d). Delivery media were supplemented with 0.2% FBS, 1% P/S, and 2 mM L-Gln. After 24 h of incubation in conditioned medium, cells were stained with calcein-AM (Invitrogen), and fluorescence images were captured using a Leica DMI3000B microscope. The total length of the tubes formed in response to VEGF was analyzed. This quantification was performed using the Angiogenesis Analyzer plugin in ImageJ software (NIH).

2.9.3. CXCL12. The functionality of CXCL12 released from SF hydrogels was examined by evaluating the migration of low-density bone marrow cells (LDBM) in response to the chemoattractant gradient of this chemokine.[30] LDBM cells were obtained from CD1 mice (Charles River Laboratories) aged 8 weeks. Under sterile conditions, the pelvic and lower (femora and tibiae) bones were removed and crushed in a porcelain mortar with PBS. The cellular content was filtered through a 100 μm cell strainer and centrifuged at 1500 rpm for 5 min. The cell pellet was resuspended in 5 mL of DMEM supplemented with 10% FBS and 1% P/S and added to 5 mL of Histopaque-1083 (Sigma-Aldrich, 10831). This solution was centrifuged at 1700 rpm without a brake for 30 min at room temperature. The white phase, containing mainly hematopoietic progenitors and other types of mononuclear cells, was aspirated. To eliminate any remaining Histopaque residues, the white phase was mixed with 40 mL of PBS and centrifuged at 1500 rpm for 5 min. The LDBM cell precipitate was dissolved in an assay medium of DMEM supplemented with 0.5% BSA and 1% P/S.

A 100 μL volume of medium containing 1×10^5 LDBM cells (input) was added to the upper chamber of a Transwell plate (Costar 3422). Control and conditional media were distributed in the lower chamber of the Transwell plate (600 μL per well). The analyzed groups were −CXCL12, +CXCL12 (10, 50, and 100 ng/mL), and +CXCL12 released from SF hydrogels at 2 and 6% with two different release time periods (0−1 and 3−7 d). Delivery media were supplemented with 1% P/S. After 4 h of incubation in the conditional media, the number of LDBM cells present in the lower chamber of the Transwell system (output) was counted.

2.9.4. TGF-β-1. The anti-inflammatory activity of TGF-β-1 released from the hydrogels was analyzed using the BV2 microglial cell line, kindly provided by Dr. Antonio Cuadrado (Instituto de Investigaciones Biomédicas Alberto Sols, Universidad Autónoma de Madrid-CSIC). BV2 cells were cultured in 24-well plates at 1×10^4 cells per well in complete medium. At a confluence of approximately 80%, BV2 cells were polarized toward a proinflammatory phenotype using *Escherichia coli* O111:B4 lipopolysaccharide (LPS, Sigma-Aldrich, L3024) at 100 ng/mL, following the procedure described by Yonesi and colleagues.[10] Cells were divided into different groups: −LPS −TGF-β-1, +LPS − TGF-β-1, +LPS + TGF-β-1 (recombinant TGF-β-1 was used at 10 ng/mL), and +LPS + TGF-β-1 released from SF hydrogels at two concentrations (2 and 6%) with two different release time periods (0−1 and 3−7 d). The control media (−LPS − TGF-β-1, +LPS − TGF-β-1, and +LPS + TGF-β-1) were composed of DMEM supplemented with 2% FBS, 1% P/S, and 2 mM l-Gln. Collected media from SF hydrogels were supplemented with 2% FBS, 1% P/S, and 2 mM L-Gln.

After 24 h of incubation in the conditioned medium, nitric oxide (NO) levels were measured using the Griess methodology. For this, culture media were treated with the Griess reagent comprising 1% (w/v) sulfanilamide (Sigma-Aldrich, S9251) in 5% (v/v) phosphoric acid and 0.1% (w/v) *N*-(1-naphthyl)ethylenediamine dihydrochloride (Sigma-Aldrich, 222488) in distilled water. The first reagent diazotizes the nitrite present in the sample, and the second converts the diazonium salt into a colored compound that can be measurable by spectrophotometry. The NO concentration in the medium was determined from absorbance measurements at 540 nm using a calibration curve.

2.9.5. Neuroprotection Induced by ISQ201. To assess the sustained biological activity of ISQ201 released from SF hydrogels, an in vitro model of ischemia-reoxygenation was performed in primary neuronal cultures subjected to oxygen and glucose deprivation (OGD) following reoxygenation. As previously described,[31] cortical neurons were cultured for 6−7 d in vitro and were then washed and placed in glucose-free culture medium (aerated with 95% N_2 and 5% CO_2 for 30 min) and kept in an anaerobic chamber (95% N_2 and 5% CO_2) at 37 °C for 4 h (OGD 4 h). After the OGD period, culture media were replaced, and cells were reoxygenated and kept in normoglycemic conditions for 24 h to recovery (R24h). At the onset of recovery, different treatments were administered, including ISQ201 at 1 or 5 μM as well as the collected media from ISQ201-SF hydrogels. After 24 h of recovery, the cell viability was assessed via the 3-(4,5-dimethylthiazol-2-yl)-2,5-diphenyl-2*H*-tetrazolium bromide (MTT) assay. Absorbance measurements were taken at 595 nm and normalized to the control group (not subjected to OGD).

2.10. Statistical Analysis. Statistical analysis was conducted using SigmaPlot v11.0 software (Systat, Germany). All results are presented as mean ± standard error of the mean (SEM). The specific statistical tests applied to every study are indicated in the corresponding figure legend. For the analysis of the mechanical properties of the hydrogels, either the *t*-Student or Wilcoxon Mann−Whitney tests were used based on the nature of the data distribution. The distribution of secondary structure and the release kinetics were assessed using Analysis of variance (ANOVA) with post hoc analysis using Tukey's test. ANOVA was used to examine the biological effects of the released molecules, followed by Dunnet's multiple comparison post hoc test. Significance was set at $p < 0.05$.

3. RESULTS

3.1. Mechanical and Structural Characterization of SF Hydrogels. SF hydrogels fabricated through an aqueous process were evaluated for their encapsulation and release of molecules with diverse characteristics. We first characterized the mechanical and structural properties of sonication-induced hydrogels. Following sonication, a loss of transparency occurs with progression of gelation due to the assembly of silk proteins

https://doi.org/10.1021/acs.biomac.4c00629
Biomacromolecules 2024, 25, 5233−5250

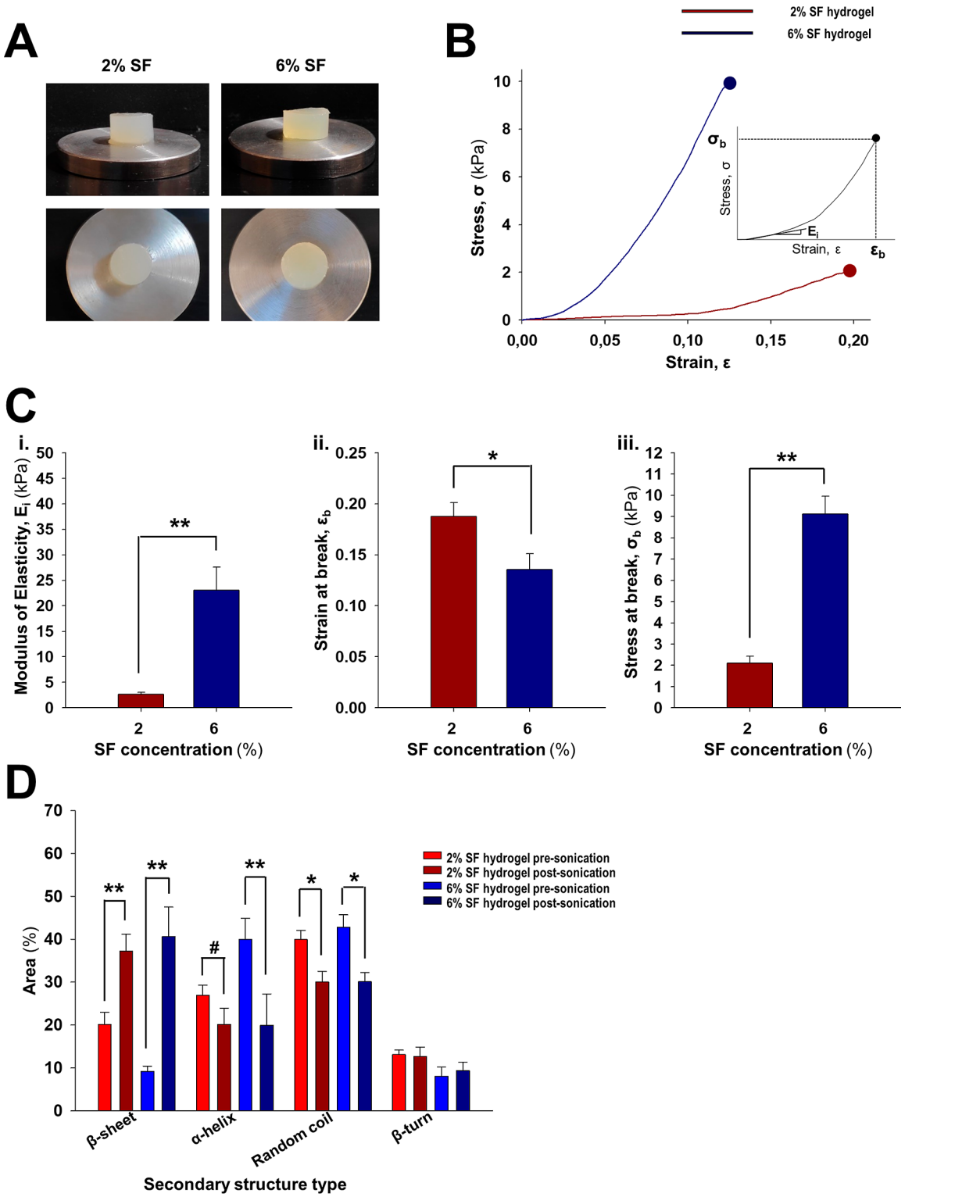

Figure 1. Mechanical and structural characterization of SF hydrogels. (A) Representative lateral and top views of SF hydrogels (2 and 6%) in PBS. (B) Representative stress (σ)−strain (ε) curves of 2 and 6% SF hydrogels. The inset depicts how the modulus of elasticity (E_i), stress at break (σb), and strain at break (εb) were calculated, with the initial modulus of elasticity being the tangent of the curve in the strain range between 1 and 3%, and the stress and strain at break being the values of these parameters at hydrogel failure, represented by the dot at the end of the curve. (C) Modulus of elasticity, strain at break, and stress at break (panels i, ii, and iii, respectively) of SF hydrogels. A minimum of nine hydrogels of each concentration were analyzed. (D) Contribution of different types of secondary structures to the total area of the amide I peak before and after sonication. A minimum of three hydrogels of each concentration were analyzed. Data are presented as mean ± standard error of the mean (SEM). Asterisks denote significant differences between the two hydrogel concentrations or between pre and postsonication states (Wilcoxon Mann−Whitney test for modulus of elasticity and stress at break, Student's *t*-test for strain at break, and ANOVA for distribution of secondary structures; *$p < 0.05$; **$p < 0.01$; and values of p between 0.1 and 0.05 are denoted with the symbol #).

https://doi.org/10.1021/acs.biomac.4c00629
Biomacromolecules 2024, 25, 5233−5250

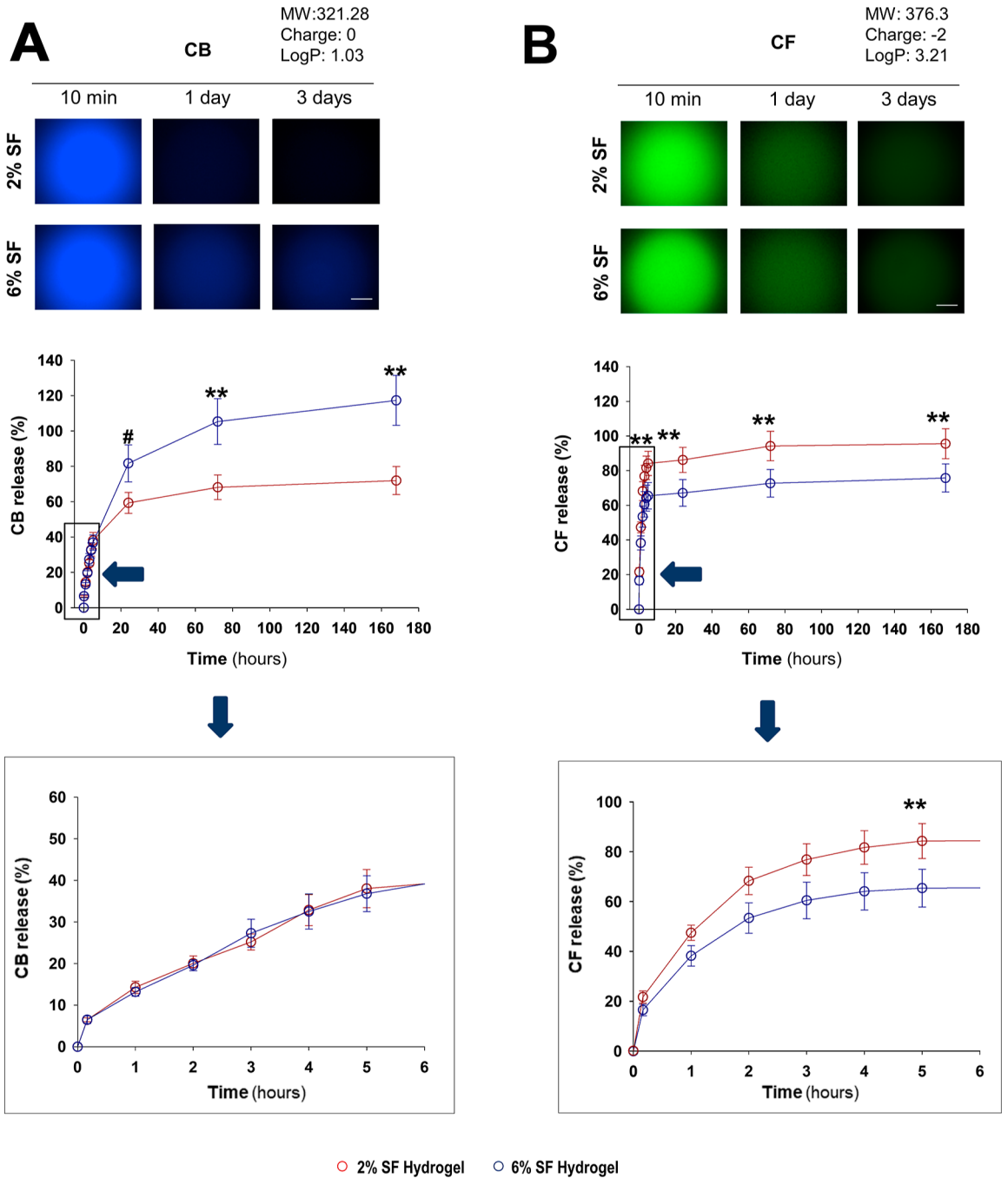

Figure 2. Release kinetics of calcein blue (CB) and carboxyfluorescein (CF) from the SF hydrogels. Top panels show representative images of SF hydrogels loaded with (A) calcein blue (CB) or (B) carboxyfluorescein (CF), at different time points after encapsulation (10 min and 1 and 3 d), denoting a progressive decay of fluorescence intensity, that was linked with the gradual delivery of fluorescent molecules (inferred from the detection of fluorescence signal in the external medium). In A and B, the middle graphs show the cumulative delivery percentage over time after encapsulation in 2 or 6% SF hydrogels. The bottom graphs show an enlargement of the delivery time course in the range from 0 to 6 h (blue arrow). The release of each molecule was analyzed from a minimum of 5−11 hydrogels per time point and SF concentration. Dark red or dark blue circles correspond to the release from 2 to 6% hydrogels, respectively. Data are presented as mean ± SEM. Asterisks denote significant differences between the two hydrogel concentrations (two-way ANOVA analysis; $^{**}p < 0.01$; and values of p between 0.1 and 0.05 are denoted with the symbol #).

into larger structures, which causes the dispersion of visible light (Figure 1A).

Two different concentrations of SF were investigated for therapeutic approaches to pharmacological release in the CNS. We selected a concentration of 2% hydrogels because the obtained hydrogels are expected to be less rigid and probably more suitable for direct administration into soft tissues such as the brain. Conversely, 6% hydrogels would create more rigid structures and would probably be more appropriate for less soft tissues such as the nasal cavity, which is a less invasive and alternative route for reaching the brain through the nasal epithelium. As expected from the composition and observed in the representative stress−strain curves in Figure 1B, the hydrogel with the highest concentration (6%) exhibited a larger elastic modulus [(Figure 1C) panel (i)] and compressive resistance [(Figure 1C) panel (iii)]. Correspondingly, the gel

https://doi.org/10.1021/acs.biomac.4c00629
Biomacromolecules 2024, 25, 5233−5250

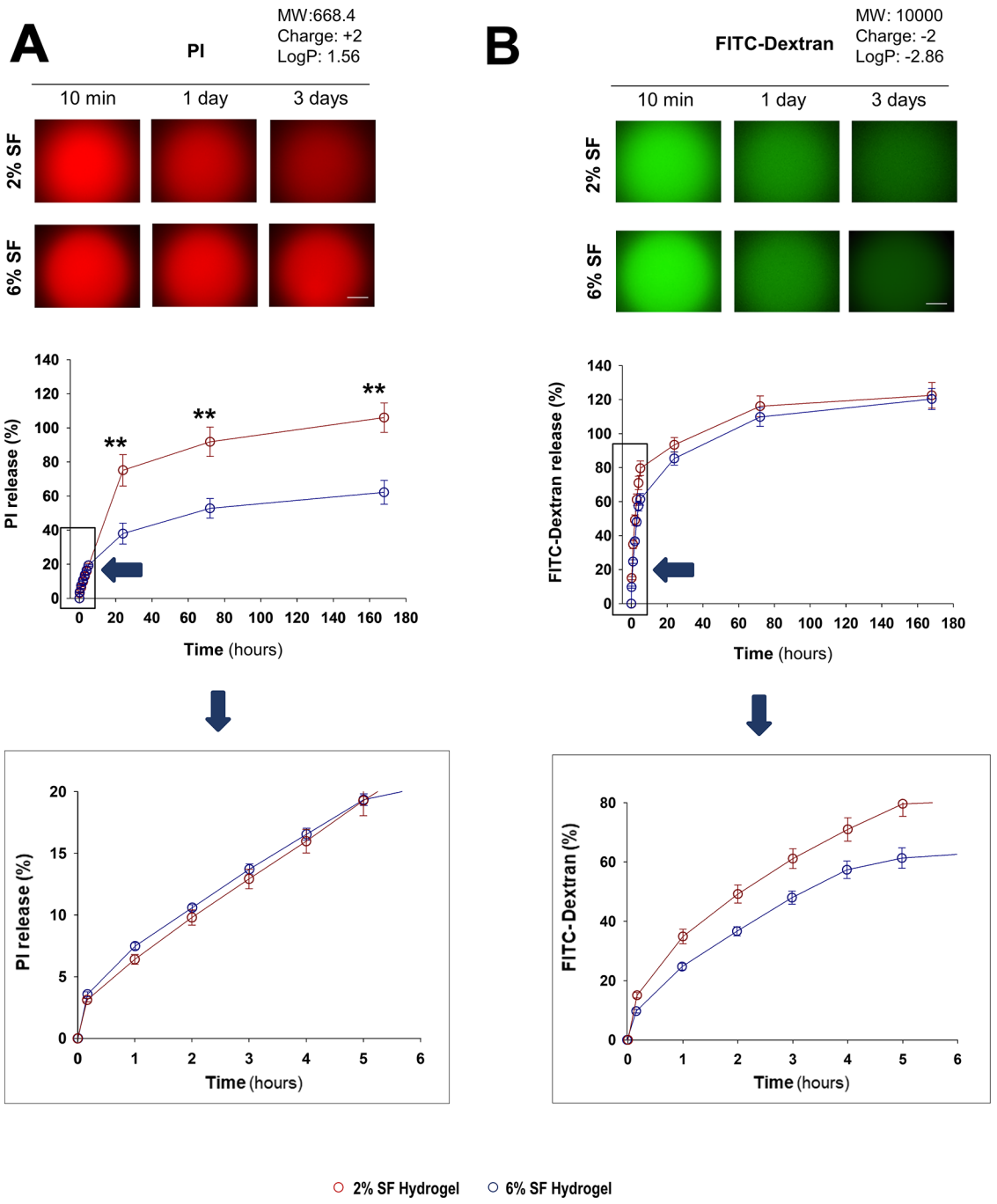

Figure 3. Release kinetics of propidium iodide (PI) and fluorescein isothiocyanate-dextran (FITC-dextran) from SF hydrogels. Top panels show representative images of SF hydrogels loaded with (A) propidium iodide (PI) or (B) fluorescein isothiocyanate-dextran (FITC-dextran), at different time points after encapsulation (10 min and 1 and 3 d), denoting a progressive decay of fluorescence intensity, that was linked with the gradual delivery of fluorescent molecules (inferred from the detection of fluorescence signal in the external medium). In A and B, the middle graphs show the cumulative delivery percentage over time after encapsulation in 2 or 6% SF hydrogels. The bottom graphs show an enlargement of the delivery time course in the range from 0 to 6 h (blue arrow). The release of each molecule was analyzed from a minimum of 5−11 hydrogels per time point and SF concentration. Dark red or dark blue circles correspond to the release from 2 to 6% hydrogels, respectively. Data are presented as mean ± SEM. Asterisks denote significant differences between the two hydrogel concentrations (two-way ANOVA analysis; $^{**}p < 0.01$).

with the lowest concentration (2%) exhibited a larger strain at breaking [(Figure 1C) panel (ii)].

The analysis of secondary structure distribution in the SF solutions (prior to sonication) and the hydrogels (24 h after sonication) was performed from the deconvolution of the amide I peak of the infrared spectra (supplementary Figure S1) following previous methodologies.[22] This analysis revealed that before gelation, the contribution of β-sheets to the total secondary structure was moderately low and did not exceed 25% (Figure 1D). However, 24 h after sonication of SF solutions, the β-sheet content of the protein significantly increased and was more pronounced in 6% hydrogels. This increase was accompanied by a parallel decrease in the number of α-helix and random coil structures. After sonication, β-sheet was the most predominant secondary structure in hydrogels (approximately 40%), followed by random coil (30%), α-helix

https://doi.org/10.1021/acs.biomac.4c00629
Biomacromolecules 2024, 25, 5233−5250

Table 3. Release Constants, Correlation Coefficients, and Akaike Information Criterion (AIC) for Korsmeyer-Peppas, Peppas−Sahlin, and Weibull Models

		CB		CF		PI		FITC-dextran	
model	parameters	2%	6%	2%	6%	2%	6%	2%	6%
Korsmeyer-Peppas	K	19.26	13.73	48.61	38.17	6.45	10.42	30.14	25.39
	n	0.31	0.61	0.47	0.44	0.66	0.36	0.54	0.56
	R^2	0.95	0.99	0.99	0.99	0.99	0.98	0.99	0.99
	AIC	51.34	16.76	7.95	12.36	8.81	48.20	5.07	18.73
Peppas−Sahlin	K_1	17.05	8.98	30.65	46.20	4.47	8.61	23.78	26.43
	K_2	−1.05	4.73	17.46	−7.07	1.98	−0.30	11.03	−1.08
	m	0.52	0.43	0.36	0.55	0.47	0.52	0.37	0.61
	R^2	0.99	0.99	0.99	0.99	0.99	0.99	0.99	0.99
	AIC	37.97	15.77	5.92	9.19	6.52	24.54	−8.90	20.45
Weibull	α	4.87	7.00	1.43	2.01	15.80	10.01	2.22	3.47
	β	0.43	0.72	0.64	0.58	0.73	0.46	0.64	0.75
	R^2	0.98	0.99	0.99	0.99	0.99	0.99	0.99	0.99
	AIC	46.79	20.99	16.79	9.99	11.75	40.14	16.62	23.32

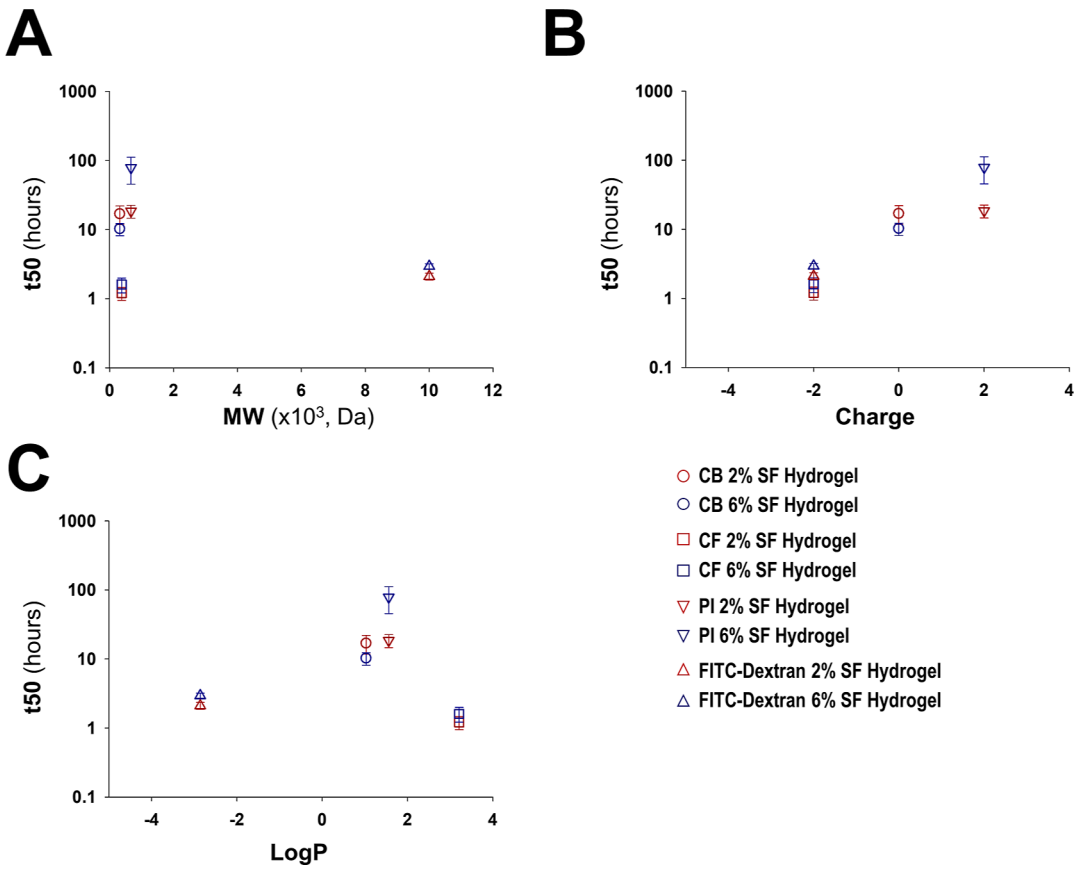

Figure 4. Relationship between t_{50} and several physicochemical properties of fluorescent molecules. Relationships between the t_{50} (extracted from the Peppas−Sahlin modeling) obtained for each fluorescent molecule and the molecular weight (MW, A), charge (B), and Log P (C) values. Different symbols are used for each molecule. At 6% SF-hydrogel concentration, negatively charged molecules tended to be released faster.

(20%), and β-turn (10%). No significant differences were found depending on SF concentration (p = 0.48; Wilcoxon Mann−Whitney).

3.2. Influence of Charge, Size, and Hydrophobicity on the Release of Molecules from SF Hydrogels. We analyzed how well hydrogel concentrations of 2 and 6% released molecules of different weights, charges, and hydrophobicities (Figures 2 and 3). All molecules were fluorescent to facilitate their detection. The delivery time course from SF hydrogels suggested distinct kinetic patterns among the four analyzed molecules. Although the four molecules were nearly completely released within the 7 d period of analysis, propidium iodide (PI), which is positively charged (+2), showed the slowest release (Figure 3A), whereas negatively charged molecules, carboxyfluorescein (CF, −2) and FITC-dextran (−2), exhibited faster release rates (Figures 2B and 3B), being slightly greater than the release curve observed for neutral calcein blue (CB) (Figure 2A). These results were consistent with the fluorescence variation inside the hydrogels (supplementary Figure S2), which had a higher retention of PI over time. The decay of

https://doi.org/10.1021/acs.biomac.4c00629
Biomacromolecules 2024, 25, 5233−5250

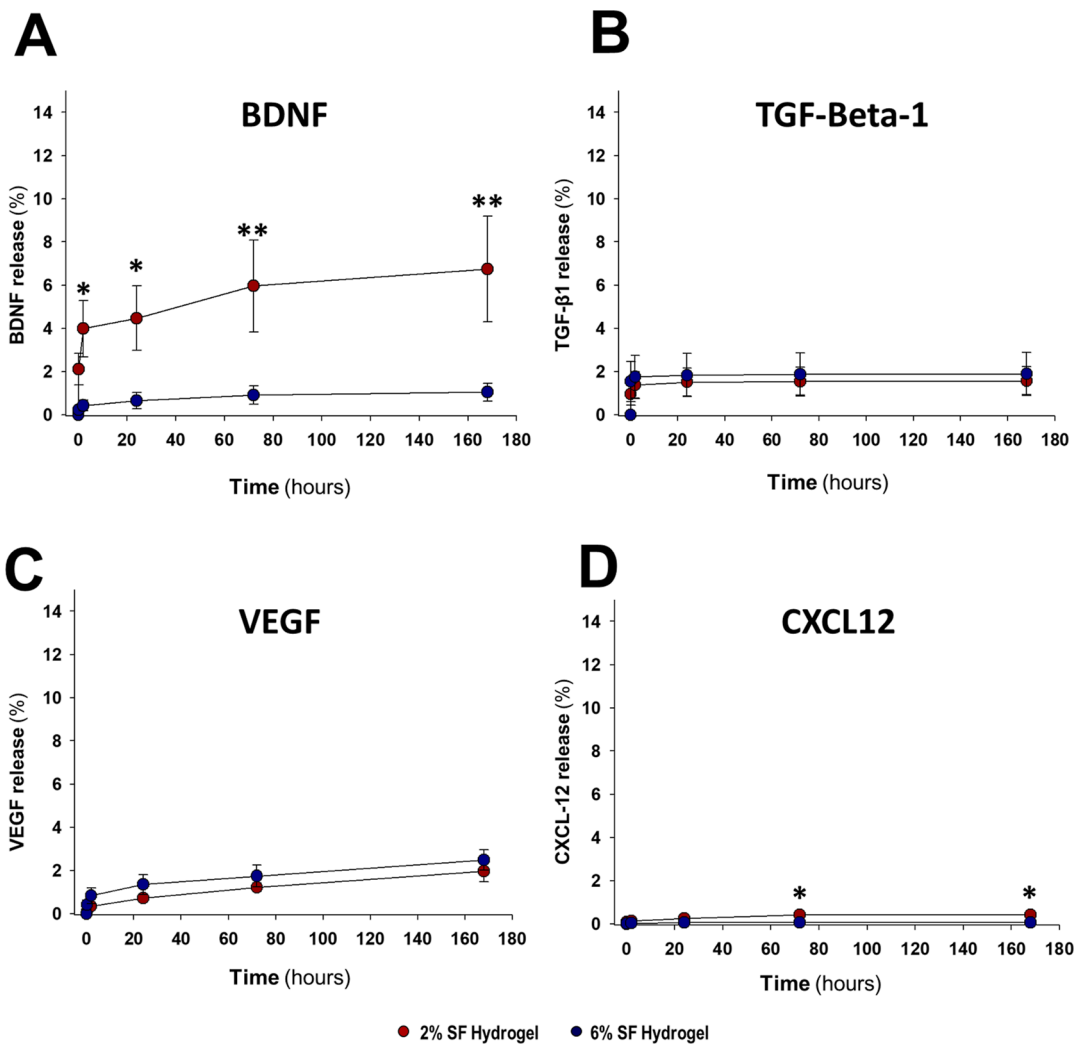

Figure 5. Release kinetics of neurovascular and anti-inflammatory factors delivered from SF hydrogels. Cumulative delivery percentage of (A) BDNF, (B) TGF-β-1, (C) VEGF, and (D) CXCL12 over 7 d after encapsulation in 2% (dark red) or 6% (dark blue) SF hydrogels. Data are presented as mean ± SEM, with 6, 5, 8, and 8 samples (hydrogels) for BDNF, TGF-β-1, CXCL12, and VEGF respectively, per SF concentration. Asterisks denote significant differences between the two hydrogel concentrations (two-way ANOVA analysis; *$p < 0.05$; and **$p < 0.01$).

fluorescence intensity inside the hydrogels probably reflected the release of molecules to the external media rather than being caused by photobleaching as the fluorescence intensity of these four molecules in PBS remained constant for at least 7 d (supplementary Figure S3).

The SF concentration in the hydrogel also seemed to influence the delivery rate. Although the release of CF and PI was significantly higher in 2% hydrogels with respect to that in 6% hydrogels (Figures 2B and 3A), the release of the neutral molecule CB (no charge) was intensified at higher polymer concentrations after the first 24 h (Figure 2A). However, no significant changes were observed in the kinetics of FITC-dextran release with different SF concentrations (Figure 3B). The delivery efficacy with regard to the biomaterial concentration was consistent with the fluorescence changes inside the hydrogel for both PI and FITC-dextran (supplementary Figure S2).

We adjusted the kinetics of delivery of the four fluorescent molecules to the theoretical models described in Methods. These models were previously used to gain insights into the mechanisms underlying the delivery of molecules from SF nanoparticles[32] or SF microparticles embedded into SF hydrogels.[33] In our study, the Peppas−Shahlin model exhibited the best fit for the majority of molecules and polymer concentrations, yielding a higher correlation coefficient R^2 and lower AIC values (Table 3). Theoretically, the better fit to the Peppas−Sahlin equation suggests a preferential mechanism of drug delivery based on a combination of Fickian diffusion (first term) and swelling or relaxation of the polymer (second term). While Fickian diffusion is produced by the diffusion of molecules due to a chemical gradient, the relaxational release (case-II transport) is a mechanism governed by the penetration of water in a glassy hydrogel matrix, which induces polymer swelling and further drug diffusion into the external releasing medium.[24] In this model, the higher value of k_1 (first term) than k_2 (second term) obtained for the majority of fluorescent molecules and SF concentrations suggests that Fickian diffusion was the predominant mechanism.

The value t_{50} that accounts for the time required to achieve a 50% release was computed for all the molecules using the Peppas−Sahlin fit and compared with their physicochemical properties (Figure 4). We did not find a discernible relationship between t_{50} and the molecular weight (explored range 0.3−10 kDa) or the hydrophobicity (log P, explored range −2.86 to

https://doi.org/10.1021/acs.biomac.4c00629
Biomacromolecules 2024, 25, 5233−5250

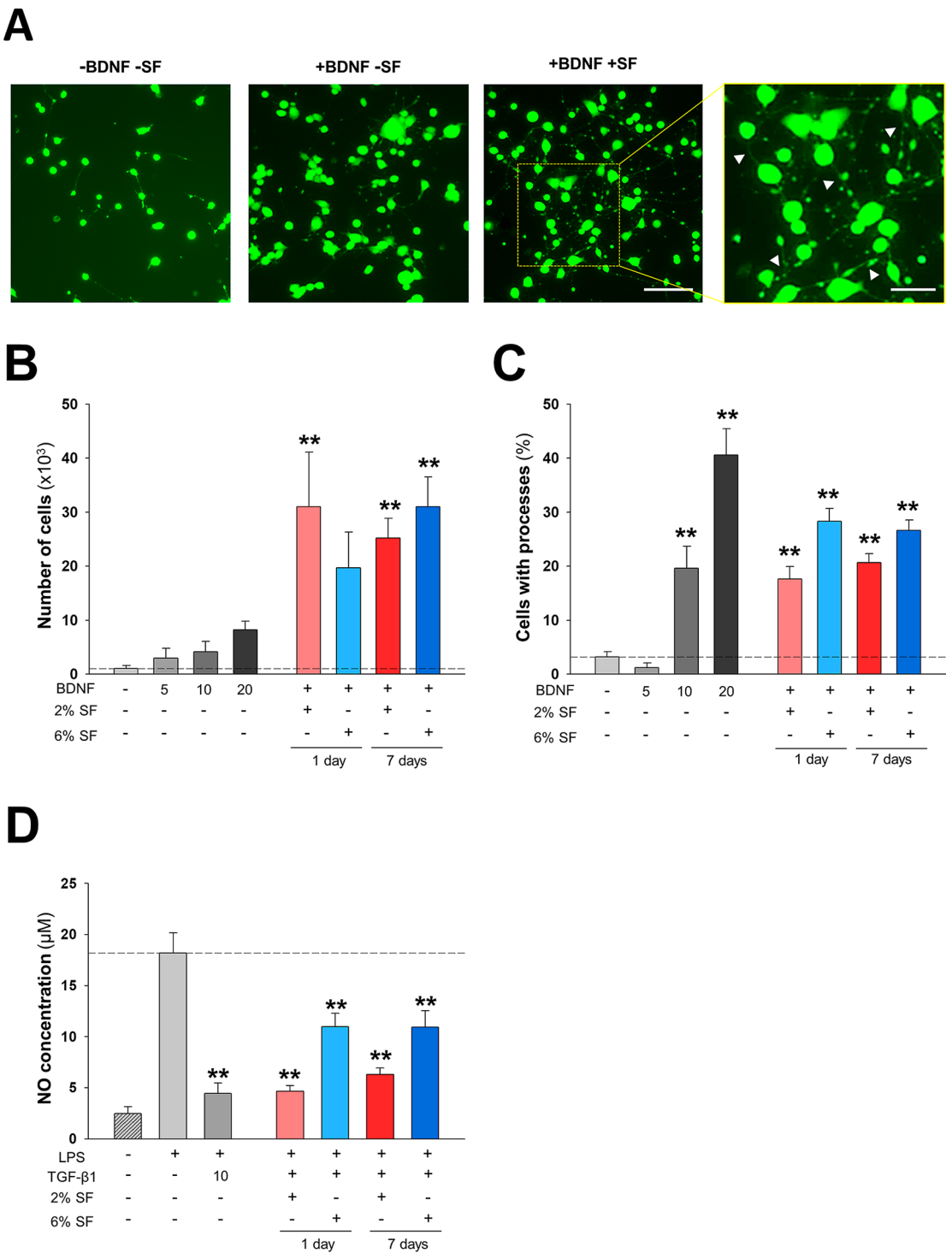

Figure 6. Biological evaluation of BDNF and TGF-β-1 released from SF hydrogels. (A) Representative images of N2A cells in the absence (negative control) or presence (positive control) of BDNF or incubated with external medium collected from BDNF-SF hydrogels (scale bar: 100 μm). The arrowheads (right panel) identify several cellular processes developed by N2A cells in response to BDNF released from SF hydrogels (scale bar: 50 μm). Quantification of cell survival (B) and percentage of N2A cells with processes (C). At least nine samples were used for control (grayscale bars) and media collected (red for 2% SF; blue for 6% SF; and at two collected time points: 1 and 7 d) groups. The dashed line indicates the biological outcome of the negative control (−BDNF). (D) Quantification of the inflammatory response of BV-2 cells classically activated (effector macrophages activated during cell-mediated immune responses) with lipopolysaccharide (LPS; a cell-mediated immune response mediator), inferred through the determination of NO concentration, in the presence of TGF-β-1 released from SF hydrogels. The biological response to TGF-β-1 was analyzed in the media derived from the release of at least six hydrogels of each SF concentration, with three replicates per release medium ($n \geq 18$). The dashed line indicates the levels of NO found in activated (+LPS) BV-2 without TGF-β-1 (negative control). All data are presented as mean ± SEM. Asterisks denote significant differences between the different groups and the control ones (−BDNF or −TGF-β-1; dashed lines) (one-way ANOVA analysis; $^{**}p < 0.01$).

https://doi.org/10.1021/acs.biomac.4c00629
Biomacromolecules 2024, 25, 5233−5250

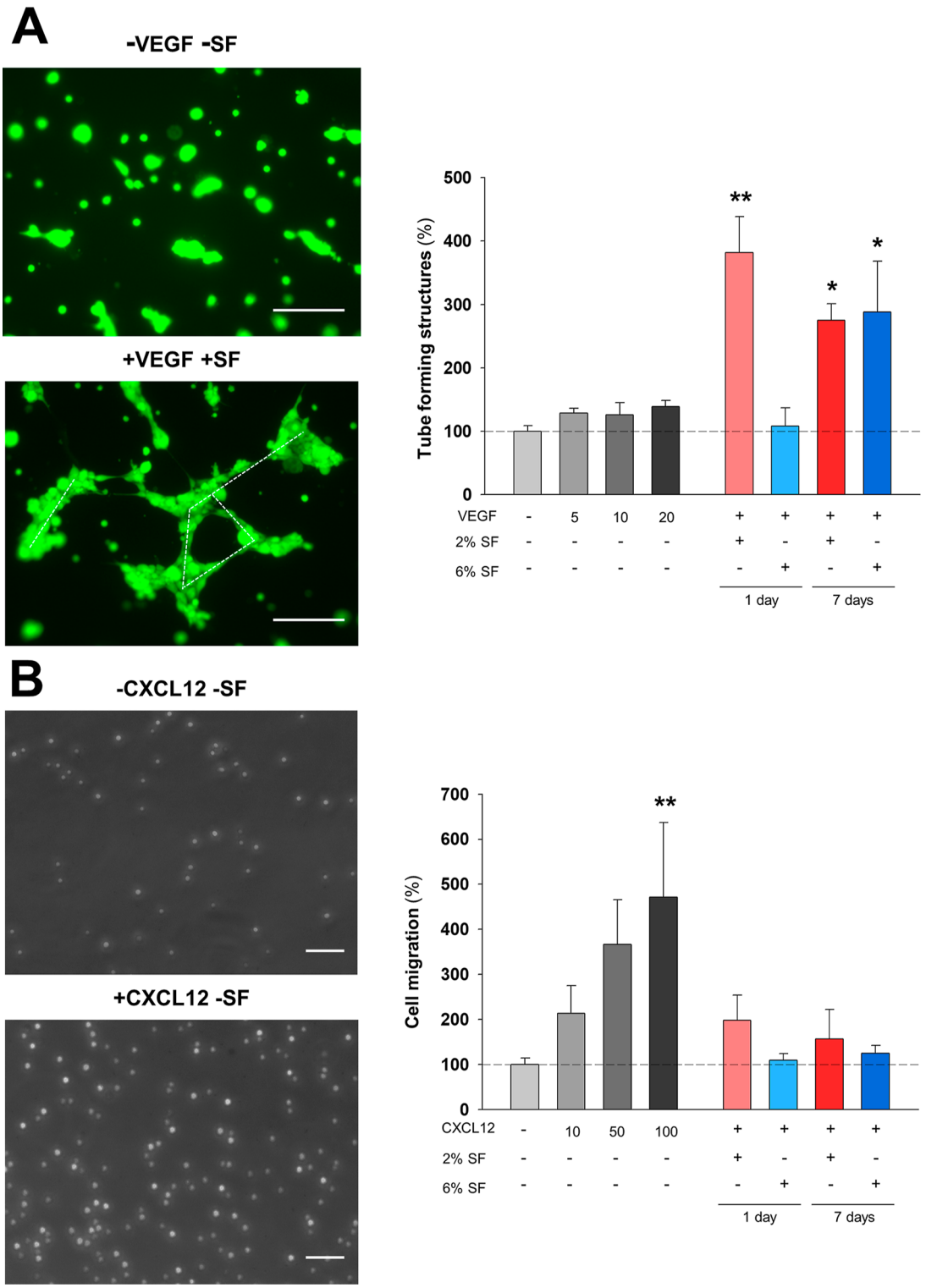

Figure 7. Biological evaluation of VEGF and CXCL12 released from SF hydrogels. (A) Left: representative images of EOMA cells in the absence (−VEGF, negative control) or the presence of VEGF released from SF hydrogels (scale bar: 200 μm). Dashed lines indicate clustering of EOMA cells into capillary-like tubular structures in response to VEGF. Right, quantification of tubes forming structures in response to VEGF released from 2 to 6% SF hydrogels at different time points of delivery. At least six samples were used for control (grayscale bars) and media collected (red tones for 2% SF; blue tones for 6% SF; and at two collected time points: 1 and 7 d) groups. The dashed line indicates the biological outcome of the negative control (−VEGF). (B) Left, representative images of LDBM cells present in the lower chamber of a Transwell (output) at the end of migration assay in the absence (top) or presence (bottom) of CXCL12 (scale bar: 50 μm). Right, percentage of LDBM cells migrated to the lower chamber. The biological response to CXCL12 was analyzed in media collected from six hydrogels of each concentration, with two replicates per release medium (n = 12). The dashed line shows the percentage of migration in the absence of CXCL12 (negative control). Asterisks denote significant differences between the different groups and the control ones (−VEGF or −CXCL12; dashed lines) (one-way ANOVA analysis; *p < 0.05; and **p < 0.01).

https://doi.org/10.1021/acs.biomac.4c00629
Biomacromolecules 2024, 25, 5233−5250

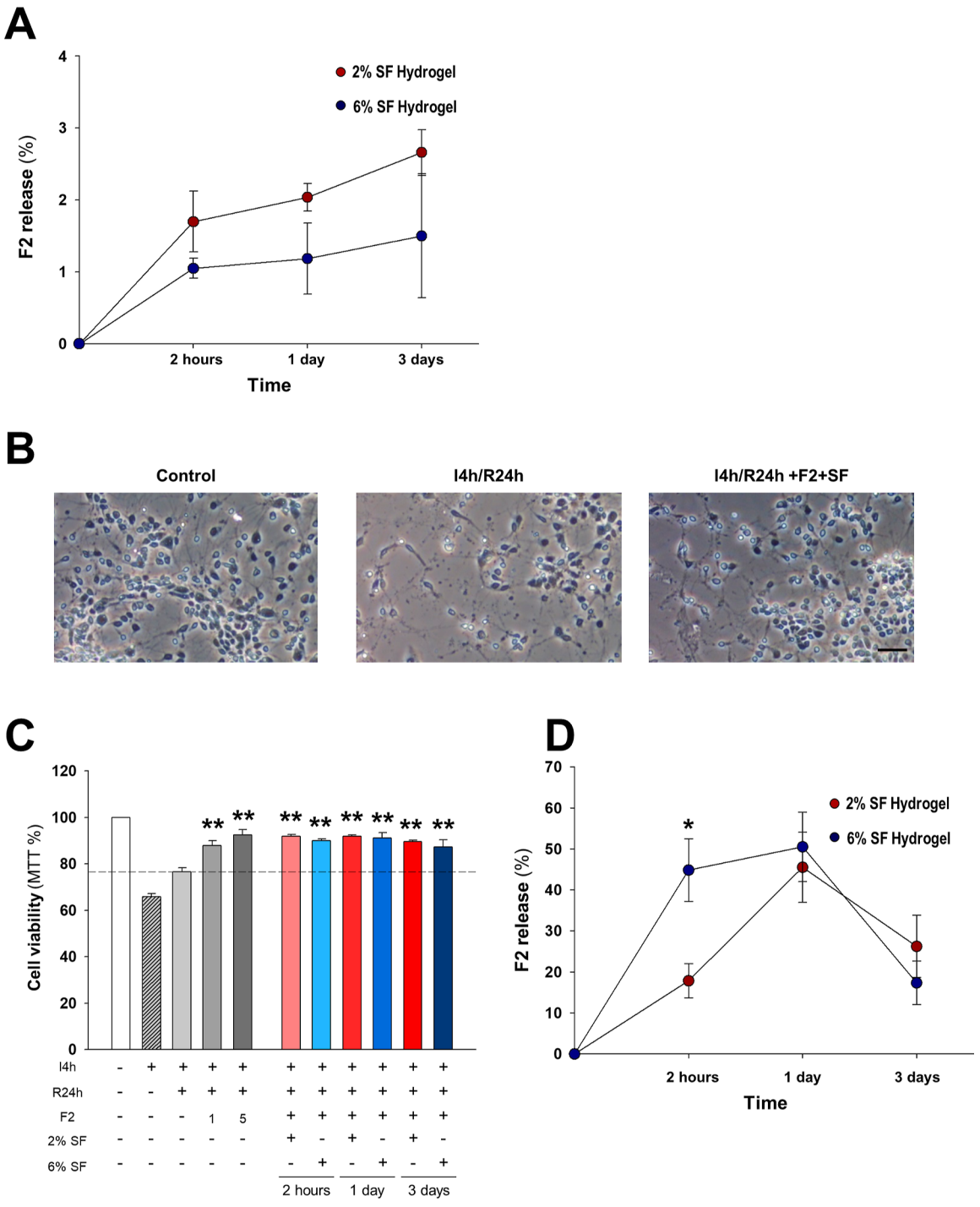

Figure 8. Time course of delivery and neuroprotective ability of nitrone ChNF2 (ISQ201) released from SF hydrogels. (A) Cumulative delivery percentage of ISQ201 (F2) in PBS along 3 days after encapsulation in 2% (dark red) or 6% (dark blue) SF hydrogels (a minimal of $n = 4$ per time point and SF concentration). (B) Representative images of primary neuron cultures in control media (left) or subjected to OGD and recovery for 24 h in the absence (middle) or presence of ISQ201 delivered from SF hydrogels (right) (scale bar: 50 μm). (C) Quantification of cell viability (MTT assay) of neurons subjected to OGD ischemia (I4h) following 24 h of recovery (R24h), and untreated or treated, at the onset of the reoxygenation period, with 1 and 5 μM ISQ201, or ISQ201 released from SF hydrogels of 2 and 6% concentration at 2 h and 1 and 3 d after encapsulation. Bar graph showing control (white), I4h (dashed gray), and I4h/R24h (clear gray) conditions, 1 and 5 μM ISQ201 treatments (gray), and treatments with ISQ201 released from 2 to 6% SF (red and blue, respectively). The dashed line shows the value (in percentage) of cell survival after ischemia-reoxygenation (I4h/R24h) without ISQ201. (D) Cumulative delivery percentage of ISQ201 in ACN−MetOH along 3 d after encapsulation in 2% (dark red) or 6% (dark blue) SF hydrogels ($n = 4$, per time point and SF concentration). Data are showed as mean ± SEM. Asterisks denote significant differences ($p < 0.01$) compared with the I4h/R24h value by Dunnett's posttest after significant ANOVA.

3.21) (Figure 4A−C). Alternatively, the charge (explored range −2 to +2) tended to influence the delivery rate, with negatively charged molecules accelerating the release, especially when this occurred from 6% hydrogels (Figure 4B).

https://doi.org/10.1021/acs.biomac.4c00629
Biomacromolecules 2024, 25, 5233−5250

Collectively, our findings indicate that SF hydrogels sustained the delivery of all tested fluorescent molecules for at least 1 week. Model fitting suggested that this gradual release could be due to the combined processes of diffusion and penetration of the solvent inside the hydrogel, coupled with polymer relaxation.

3.3. Delivery of Therapeutic Factors from SF Hydrogels. We then analyzed the functional capacity of SF hydrogels to deliver molecules with therapeutic outcomes for brain pathologies. We screened four protein factors with neuroprotective, angiogenic, chemoattractant, and anti-inflammatory properties (BDNF, VEGF, CXCL12, and TGF-β-1, respectively). These four molecules have been previously tested without any biomaterial-based delivery system in the context of different cerebral pathologies, aiming either to reduce the extent of damage or to promote brain tissue regeneration. In a previous report, we found that encapsulation of mesenchymal stem cells (MSCs) in SF hydrogels impaired the MSC fitness, and with the exception of TGF-β-1, we found an altered secretion of BDNF, VEGF, and CXCL12.[34] To bypass this stem cell−secretome deficit, which may be related to the compartmentalization of this cell population inside the hydrogel, we explored the potential of the biomaterial to deliver these factors directly encapsulated within the hydrogel.

We first noticed that these four molecules were unstable in a saline solution (supplementary Figure S4). After 24 h of incubation in PBS at 37 °C, no more than 20% of the initial concentration of VEGF, CXCL12, or TGF-β-1 could be detected via ELISA (supplementary Figure S4). BDNF demonstrated relatively higher stability, with approximately 40% detectable after 24 h, but became undetectable after 7 days in solution (supplementary Figure S4).

After their reconstitution with the hydrogel, all of these factors were delivered and detected by ELISA in the external medium. The release curves indicated a percentage of delivery inferior to 6% for most molecules within a 7 d interval, with CXCL12 being the factor that was released to a lesser extent (Figure 5). We found that higher concentrations of SF (6%) decreased the amount of BDNF and CXCL12 delivered to the external media, whereas changes in polymer concentration did not significantly influence the release rates of VEGF and TGF-β-1.

To confirm the functionality of the encapsulated molecules and their sustained delivery from the hydrogel, we used specific cell culture assays to analyze the effects of the external media collected at different time points after encapsulation (Figures 6 and 7). Because all four factors exhibited a low rate of delivery (Figure 5), in these assays, the amount of uploaded molecules was subsequently increased in the scaffold.

With the exception of the external media taken from CXCL12 hydrogels, which did not exhibit any chemoattractant effect at any of the analyzed release time points (Figure 7B), the other three molecules demonstrated varying degrees of functionality in each specific cell model. For instance, media collected from BDNF-SF hydrogels enhanced survival (Figure 6A,B) and the number of cellular processes of the neural cell line N2A (Figure 6C). TGF-β-1 delivered from hydrogels attenuated the inflammatory response, as evidenced by a reduction in the inflammatory levels of NO secreted by the BV2 microglial cell line after LPS activation (Figure 6D). VEGF stimulated the rearrangement of an endothelial cell line (EOMA) into tubelike structures on Matrigel, which is indicative of angiogenesis (Figure 7A). The biological activities of BDNF, TGF-β-1, and VEGF were also observed at later time points, as these factors exerted a clear functional effect when the external medium was collected 7 days after encapsulation. Thus, the SF hydrogel may preserve and stabilize the functional activity of these protein factors.

We next assessed the efficacy of the SF scaffold to deliver ISQ201, a promising small (MW: 413.36 Da) molecule that has demonstrated significant antioxidant properties in animal models of transient and permanent cerebral ischemia.[26,35] In vivo, this molecule has a limited half-life of <2 h when administered intravenously.[26b] In comparison with the small fluorescent molecules previously analyzed (Figures 2 and 3), the release of ISQ201 from SF hydrogels within an equivalent period was considerably lower (Figure 8A), not exceeding a 3% release of the total ISQ201 encapsulated in 3 d. Although the release of ISQ201 from 6% hydrogels was slightly lower than that from 2% hydrogels, this difference was not statistically significant.

Given the limited release of ISQ201 from the SF hydrogels, we questioned whether this biomaterial in the hydrogel format would preserve the functionality of this molecule, thereby exerting a sustained effect. To evaluate this, ischemia-reoxygenation experiments were performed to examine the viability of neuronal cell cultures at 4 h of OGD, followed by 24 h of recovery. Media collected from ISQ201-SF hydrogels of 2 and 6% at time points of 2 h and 1 and 3 d were analyzed for ISQ201 content by mass spectrometry (supplementary Figures S5 and S6) and assayed for neuroprotection induction of neurons after OGD. All the collected media, containing approximately 4 μM of ISQ201 in the case of 2% SF and 2 μM in the case of 6%, regardless of the collection time point and SF concentration, increased cell viability of neurons subjected to OGD (Figure 8B,C) and reached, in most cases, the neuroprotection values found in treated groups with compound ISQ201 at 1 and 5 μM (Figure 8C).

The release of small (<1 kDa) fluorescent molecules from SF hydrogels (Figures 2 and 3) did not seem to depend on the degree of hydrophobicity of the encapsulated molecules in the approximate Log P range from −3 to +3. Nevertheless, ISQ201 is a highly hydrophobic molecule (Log P = 8), whose release toward an aqueous medium such as PBS could be conditioned by its interaction with SF, a highly hydrophobic protein.[36] Therefore, the release kinetics of ISQ201 from SF hydrogels exposed to an organic solution of ACN−MeOH was analyzed (Figure 8D). Interestingly, the delivery of ISQ201 under these conditions was significantly greater than that for the delivery toward PBS (Figure 8A), reaching delivery percentages close to 20−50% in a similar period of 3 d. This observation emphasizes the effect of the external media composition in the release of highly hydrophobic biomolecules from SF hydrogels.

4. DISCUSSION

Currently, new drug carrier systems are urgently required to treat brain diseases by maintaining therapeutic concentrations of molecules throughout the required treatment duration. The bottlenecks that prevent the use of biomaterial-based delivery systems in the clinical setting and the area of neurology are multifactorial. They likely include a lack of precise knowledge about the optimal treatment window duration, a lack of control of biomaterial degradability that could be adjusted to this time window, and concerns of biocompatibility of biomaterial grafts and possible byproducts generated during treatment. In addition, drug delivery in most preclinical studies is mostly controlled by the biomaterial itself as concentrations of therapeutic molecules do not change dynamically in response to pathological environment signal variations.

https://doi.org/10.1021/acs.biomac.4c00629
Biomacromolecules 2024, 25, 5233−5250

The local delivery of therapeutic molecules from natural and synthetic biomaterials constitutes a highly promising yet poorly exploited approach to precision medicine, especially in clinical neurology. Among the various widely developed and characterized biomaterial formats, in situ forming hydrogels hold a particular relevance because they can be injected in liquid form and subsequently gel within the tissue.[37] These in situ forming hydrogels minimize tissue damage during the injection procedure and allow the biomaterial to conform to the tissue geometry. This relevance is emphasized in applications that require sustained delivery of therapeutic molecules over short and prolonged times. For instance, after a brain stroke, this approach may be employed to neuroprotect the brain during the acute phase or to stimulate brain plasticity and perilesional reorganization linked with recovery during the subacute and chronic stages. In comparison with systemic administrations, the local delivery of drugs may help to prevent undesired effects outside of the brain.

This study significantly increased our knowledge of the capacity of SF hydrogels, which had been fabricated through an aqueous process, to sustain the delivery of different molecules of distinct physicochemical characteristics. Importantly, the sonication approach that was used in this work proved to be an optimal method for SF-hydrogel gelation, avoiding the need for drastic changes in pH, temperature, and UV irradiation. Unlike other methods, sonication involves the formation of ultrasonic waves inside the pure aqueous SF solution and does not introduce additional molecules. This simplicity makes sonication an attractive option for biomedical applications, especially in drug delivery, where maintaining the stability of incorporated proteins and their biocompatibility are crucial.

Our results do not support a possible influence of size (explored molecular weight: range 0.3 to 10 kDa) or hydrophobicity (explored Log *P*: range −2.86 to 3.21) on the release of the four selected fluorescent molecules in PBS. However, very hydrophobic molecules such as the antioxidant molecule ISQ201 (Log *P* close to 8.0) were mostly retained inside the SF hydrogel when the external medium was composed of PBS. When this medium was replaced by a hydrophobic solvent (ACN−MeOH), the release rate of ISQ201 was substantially superior. Although we cannot generalize this observation, this result agrees with some previous literature studies[9a] and highlights the hydrophobic nature of SF protein sequences, which can limit the delivery of compounds, especially when they are highly hydrophobic.

Previously, we have found a marked resistance of SF hydrogels to degradation in saline solutions.[10] Under these pseudophysiological conditions (PBS) and along 7 days of analysis, we found that the SF hydrogel weight, and the secondary structure (β-sheet content) quantified by ATR-FTIR, remained constant, and both parameters were only impaired by enzymatic digestion (proteinase K). This result agrees with previous observations, where the deswelling ratio of SF hydrogels (inferred from the analysis of weight) in PBS was negligible,[38] suggesting that the mechanism driving the delivery of molecules from pure SF hydrogels in PBS is unlikely to be due to progressive matrix erosion or changes in secondary structure. In addition, the best fit to the Peppas−Sahlin model and a higher value of the k_1 parameter compared with the k_2 parameter suggest that drug delivery from this specific biomaterial format is mainly due to Fickian diffusion, with a marginal contribution of the polymeric chain relaxation (case II transport). In fact, for the majority of formulations, the negative values of k_2 found in our study suggests that case-II relaxational release contribution was almost absent.[39]

We also showed that SF hydrogels sustain, for at least 1 week, the delivery of several protein factors, namely, BDNF, VEGF, CXCL12, and TGF-β-1. BDNF has shown a critical role in neuronal survival and plasticity.[40] VEGF is the main mitogenic agent that stimulates cerebral angiogenesis, which is essential to promote postischemic revascularization and neuronal rewiring in perilesional areas.[41] TGF-β-1 is a cytokine involved in regulating the inflammatory state of different cell types in the brain and exerts anti-inflammatory effects promoting neuroprotection after cerebral injury and neurodegeneration.[42] CXCL12, a chemotactic cytokine, has shown relevant roles in cerebral injury, including the modulation of inflammation, angiogenesis, and the recruitment of different stem cell and progenitor populations to the area of injury.[43] All four of these factors share a common low in vivo stability in physiological fluids and reduced capacity to cross the BBB and reach the brain after systemic administration. In addition, several of these molecules, such as VEGF, have been associated with significant side effects when administrated systemically or intracerebrally, causing the opening of BBB and inducing cerebral edema.[44]

One cause of protein instability is protein aggregation, which occurs even in physiological solutions, with thermodynamically favored conditions such as neutral pH and 37 °C.[45] Except for CXCL12, the other three factors released from SF hydrogels exerted noticeable functional effects even when delivered 7 days after encapsulation. This observation suggests that SF hydrogels preserve their functional activity, e.g., by decreasing protein aggregation and thereby enhancing protein stability. This argument is supported by the hydrophobic nature of SF that may improve protein physical stability by shielding the exposition of hydrophobic domains of proteins reconstituted in this biomaterial, thus preventing protein-to-protein aggregation.[46]

However, we also found that the amount of CXCL12 delivered from SF hydrogels was extraordinarily low, with a null biological effect. This observation contrasts with the high delivery of CXCL12-FITC complexes (determined by fluorescence signal measurement) from SF hydrogels, whose gelation was induced by the addition of ethanol, although the functional implication of this delivery was not addressed.[18] The process of hydrogel fabrication (addition of ethanol versus sonication in our case) and the method of measurement (fluorescence versus ELISA in our case) may explain these discrepancies. Interestingly, all four fluorescent molecules, even those with molecular sizes similar to those of the protein factors assayed (i.e., FTIC−dextran), were delivered nearly completely from the hydrogels over 7 d. This contrasted with the generally reduced delivery rates, determined by ELISA, of the four cytokines and growth factors tested in our study. This lower delivery efficacy was surprisingly accompanied by a significant biological activity in the delivery medium of BDNF, VEGF, and TGF-β-1 samples, indicating a possible underestimation of the real content of these protein factors as determined by ELISA. Due to this fact, and since the concentration of these four trophic factors, quantified by ELISA, considerably declined over time in PBS (supplementary Figure S4), we believe that the delivery rate of these four factors does not reflect a pure release mechanism, and their reduced stability might contribute to distort their release curve. Despite this limitation, we believe that the kinetic study with fluorescent molecules has provided relevant information on the mechanisms of delivery from SF hydrogels,

https://doi.org/10.1021/acs.biomac.4c00629
Biomacromolecules 2024, 25, 5233−5250

which were mostly based on Fickian diffusion, and with a theoretical contribution of the net charge present in each molecule.

We also showed for the first time that SF hydrogels can deliver an antioxidant scavenger molecule, the nitrone ISQ201. Although the cumulative delivery of ISQ201, as determined by MALDI-TOF mass spectrometry, was <2.5−3% 3 d after encapsulation, we showed that the ISQ201 present in the delivery medium (between 2 and 4 μM of ISQ201 in 2 and 6% SF hydrogels, respectively; data not shown) exerted significant neuroprotection in a model of ischemia-reoxygenation. As commented above, the efficacy of delivery significantly increased when the external medium (PBS) was replaced by a mix of ACN−MeOH, suggesting that the poor release of ISQ201 from SF hydrogels in aqueous medium is probably due to an intense interaction of this molecule with hydrophobic residues present in the SF backbone. The hydrophobic amino acid motif GAGAGS, extensively found in the primary sequence of SF, accounts for the hydrophobic nature of this biomaterial.[47] Previous studies on SF hydrogels loaded with IgG1 antibodies reported that the external media composition can affect the delivery of molecules. For instance, the surfactant polysorbate 80 interfered with silk-antibody hydrophobic interactions, facilitating antibody release from the hydrogel.[9a] We believe that highly hydrophobic molecules such as ISQ201 may strongly interact with hydrophobic residues of the SF imposing delivery restrictions not observed with less-hydrophobic molecules. The use of hydrophobic solvents such as ACN−MeOH might disrupt these interactions, increasing the delivery efficacy. Therefore, our data suggest that not only diffusion but also external media composition and solvent penetration can influence the rate of delivery of molecules from SF hydrogels. The use of nitrones in clinical research is very promising in many diseases relating with aging such as stroke, neurodegeneration, and cancer, which are known to enhance levels of free radicals and oxidative stress. Antioxidant nitrones such as ISQ201 are in general unstable. For example, ISQ201 has a reportedly limited half-life in vivo restricted to 1.5−2 h after intravenous administration.[26b] Oxidative stress induces delayed neuronal death following brain ischemia, and oxidative changes are reported during acute stroke as early as 2−8 h, persisting even 48 h postischemia in humans.[48] This suggests a therapeutic time window opportunity larger than the stability of many antioxidant molecules. Thus, although low efficacy of delivery toward polar solvents was evident, our results are compatible with an extended temporal stability of ISQ201 using a SF hydrogel—based approach, which have repercussion to target diseases associated with inflammation and oxidative stress.

The concept of using SF as a vehicular system to deliver therapeutic molecules is not new. This biomaterial has been previously employed mostly to deliver small chemotherapeutic drugs such as doxorubicin or vincristine,[38] antibiotics, anti-inflammatory molecules (e.g., dexamethasone or prednisone), and antibodies.[9c] With the exception of CXCL12,[18] the capacity of SF hydrogels alone to directly deliver BDNF, VEGF, and TGF-β-1 had not been previously explored, although BDNF and VEGF have been administrated from other biomaterial hydrogels. For example, an in situ gelling hyaluronic acid hydrogel was used to deliver VEGF in the stroke cavity inducing changes in neural and vascular networks that caused behavioral improvement.[49] Interestingly, a pH-sensitive peptide nanofiber-based self-assembling hydrogel with arginine−alanine−aspartic repetitions was used to deliver VEGF and angiopoietin-1 after experimental stroke. This strategy promoted neovascularization and neuronal survival in areas surrounding the infarct core with a significant recovery of sensorimotor function.[50] BDNF has been intracerebrally delivered from hyaluronan hydrogels in both rodent and nonhuman primates after stroke; in rodents, this hydrogel sustained the delivery of BDNF for over 3 weeks, leading to behavioral recovery.[51] Despite the strength of this preclinical evidence, no clinical trials have been performed to support the therapeutic use of biomaterial-based strategies to control drug delivery in the brain. This may be attributed to a lack of consensus on the most suitable biomaterial or the absence of trials focused on evaluating the toxicity of implants and comprehensive pharmacokinetic profiles. Information is also lacking on the required treatment duration and therapeutic windows for neuroprotection in humans during the acute phase or remodeling/plasticity in subacute and chronic phases and whether this window is translatable as important differences exist between in vivo models (typically rodents) and human time scales.[52] In addition, drug delivery is usually not controllable once the biomaterial has been implanted. Several advanced strategies (4D smart scaffolds) have been developed to externally (e.g., with magnetic fields) or internally (in response to brain pathological signals) control this delivery. For instance, several studies have used pH- or magneto-responsive hydrogels based on Salecan,[53] hyaluronan,[50] or even SF.[54] Moreover, in a previous study, ultrasound waves enhanced the release rate of the anticancer drug vincristine from SF hydrogels, which correlated very well with a multiphysics computational model based on pressure-acoustic, diffusion, and mechanical behaviors.[55]

5. CONCLUSIONS

This study expands the list of in situ forming hydrogels that can sustain the delivery of therapeutic compounds for biomedical and specific neurological applications. First, SF hydrogels were able to nearly completely deliver four fluorescent molecules of different sizes (explored range 0.3−10 kDa), hydrophobicity (log P, explored range −2.86 to 3.21), and charge (explored range −2 to +2). The theoretical modeling suggests that this delivery was mainly driven by Fickian diffusion with a marginal contribution of relaxation of the polymer (case-II transport). The net charge of each molecule also influenced the delivery process as negatively charged molecules such as carboxyfluorescein and FITC−dextran tended to be delivered faster. Second, we have demonstrated that SF hydrogels preserved, for at least 7 days, the functional capacity of three different protein factors (BDNF, TGF-β-1, and VEGF) and one antioxidant molecule (ISQ201), all of them with very reduced stability in PBS at 37 °C (pseudophysiological conditions). In addition, the low delivery of ISQ201 in PBS was dramatically increased by changing the external media composition from PBS to the solvent ACN−MeOH, suggesting that very hydrophobic molecules can be strongly trapped in the SF backbone structure, thus limiting their delivery. Although SF is absorbable under certain conditions, SF is characterized by slow degradation, especially in the nervous system. This makes this biomaterial particularly suitable for the sustained release of factors that can induce brain remodeling after sudden brain damage, a process that although not yet fully established would require long-treatment periods that involve the progressive formation of new vasculature and neural rewiring in perilesional areas to support brain function restoration. Our results support the development of advanced vehicles of SF for

https://doi.org/10.1021/acs.biomac.4c00629
Biomacromolecules 2024, 25, 5233−5250

the delivery of protein factors and neuroprotective molecules to treat brain pathologies.

■ ASSOCIATED CONTENT

Data Availability Statement

FTIR spectra of silk fibroin solutions and hydrogels and representative mass spectrometry spectra for the quantification of cholesteronitrone ISQ201 are available (Open Access) at R.F.-S., A.L., L.P., M.Y., A.A., M.C., J.M.-C., J.P.-R., F.J.R., F.P., G.V.G., and D.G.-N. database from permselectivity of silk fibroin hydrogels for advanced drug delivery neurotherapies [data set]. Zenodo.org. 2024. 10.5281/zenodo.11071240 (accessed on 26 April 2024). The remaining data of this study are available from the corresponding author upon reasonable request.

Supporting Information

The Supporting Information is available free of charge at https://pubs.acs.org/doi/10.1021/acs.biomac.4c00629.

FTIR spectra of SF in solution or hydrogel, fluorescent molecules retention inside SF hydrogels, stability of the fluorescent molecules, stability of the protein factors, and mass spectrometry spectra (PDF)

■ AUTHOR INFORMATION

Corresponding Author

Daniel González-Nieto − *Center for Biomedical Technology, Universidad Politécnica de Madrid, Pozuelo de Alarcón 28223, Spain; Silk Biomed SL, Galapagar 28260, Spain; Centro de Investigación Biomédica en Red de Bioingeniería, Biomateriales y Nanomedicina (CIBER-BBN), Instituto de Salud Carlos III, Madrid 28029, Spain; Departamento de Tecnología Fotónica y Bioingeniería, ETSI Telecomunicaciones, Universidad Politécnica de Madrid, Madrid 28040, Spain;* orcid.org/0000-0003-2972-729X; Phone: (+34) 910679280; Email: daniel.gonzalez@ctb.upm.es

Authors

Rocío Fernández-Serra − *Center for Biomedical Technology, Universidad Politécnica de Madrid, Pozuelo de Alarcón 28223, Spain; Silk Biomed SL, Galapagar 28260, Spain;* orcid.org/0000-0002-7362-117X

Amira Lekouaghet − *Center for Biomedical Technology, Universidad Politécnica de Madrid, Pozuelo de Alarcón 28223, Spain*

Lorena Peracho − *Department of Research, Hospital Universitario Ramón y Cajal, Madrid 28034, Spain; Proteomics Unit, Instituto Ramón y Cajal de Investigación Sanitaria (IRYCIS), Madrid 28034, Spain*

Mahdi Yonesi − *Center for Biomedical Technology, Universidad Politécnica de Madrid, Pozuelo de Alarcón 28223, Spain*

Alberto Alcázar − *Department of Research, Hospital Universitario Ramón y Cajal, Madrid 28034, Spain; Proteomics Unit, Instituto Ramón y Cajal de Investigación Sanitaria (IRYCIS), Madrid 28034, Spain;* orcid.org/0000-0002-7904-481X

Mourad Chioua − *Laboratory of Medicinal Chemistry, Institute of General Organic Chemistry (CSIC), Madrid 28006, Spain*

José Marco-Contelles − *Laboratory of Medicinal Chemistry, Institute of General Organic Chemistry (CSIC), Madrid 28006, Spain; Center for Biomedical Network Research on Rare Diseases (CIBERER), CIBER, ISCIII, Madrid 28029, Spain*

José Pérez-Rigueiro − *Center for Biomedical Technology, Universidad Politécnica de Madrid, Pozuelo de Alarcón 28223, Spain; Silk Biomed SL, Galapagar 28260, Spain; Departamento de Ciencia de Materiales, ETSI Caminos, Canales y Puertos, Universidad Politécnica de Madrid, Madrid 28040, Spain; Centro de Investigación Biomédica en Red de Bioingeniería, Biomateriales y Nanomedicina (CIBER-BBN), Instituto de Salud Carlos III, Madrid 28029, Spain; Biomaterials and Regenerative Medicine Group, Instituto de Investigación Sanitaria del Hospital Clínico San Carlos (IdISSC), Calle Prof. Martín Lagos s/n, Madrid 28040, Spain*

Francisco J. Rojo − *Center for Biomedical Technology, Universidad Politécnica de Madrid, Pozuelo de Alarcón 28223, Spain; Silk Biomed SL, Galapagar 28260, Spain; Departamento de Ciencia de Materiales, ETSI Caminos, Canales y Puertos, Universidad Politécnica de Madrid, Madrid 28040, Spain; Biomaterials and Regenerative Medicine Group, Instituto de Investigación Sanitaria del Hospital Clínico San Carlos (IdISSC), Calle Prof. Martín Lagos s/n, Madrid 28040, Spain*

Fivos Panetsos − *Silk Biomed SL, Galapagar 28260, Spain; Biomaterials and Regenerative Medicine Group, Instituto de Investigación Sanitaria del Hospital Clínico San Carlos (IdISSC), Calle Prof. Martín Lagos s/n, Madrid 28040, Spain; Neurocomputing and Neurorobotics Research Group, Faculty of Biology and Faculty of Optics, Universidad Complutense de Madrid, Madrid 28040, Spain*

Gustavo V. Guinea − *Center for Biomedical Technology, Universidad Politécnica de Madrid, Pozuelo de Alarcón 28223, Spain; Silk Biomed SL, Galapagar 28260, Spain; Departamento de Ciencia de Materiales, ETSI Caminos, Canales y Puertos, Universidad Politécnica de Madrid, Madrid 28040, Spain; Centro de Investigación Biomédica en Red de Bioingeniería, Biomateriales y Nanomedicina (CIBER-BBN), Instituto de Salud Carlos III, Madrid 28029, Spain; Biomaterials and Regenerative Medicine Group, Instituto de Investigación Sanitaria del Hospital Clínico San Carlos (IdISSC), Calle Prof. Martín Lagos s/n, Madrid 28040, Spain*

Complete contact information is available at: https://pubs.acs.org/10.1021/acs.biomac.4c00629

Author Contributions

R.F.-S. and A.L. authors contributed equally to this work. G.V.G. and D.G.-N. conceived the idea and supervised the whole project. R.F.-S. and A.L. performed the majority of the experiments with the help of M.Y. L.P. and A.A. performed the quantification of ISQ201 by mass spectrometry and the neuroprotection assays. M.C. and J.M.-C. prepared and provided ISQ201 (ChNF2). J.P.-R., F.J.R., and F.P. provided crucial designs and protocols for biomaterial fabrication and characterization. A.L., R.F.-S., and D.G.-N. wrote the paper with input from all authors.

Notes

The authors declare no competing financial interest.

■ ACKNOWLEDGMENTS

We thank Soledad Martinez for the excellent technical assistance and Alejandro Escobar-Peso for his assistance in neuronal culture experiments. This study was partially funded by the Ministerio de Ciencia e Innovación (PID2020-116403RB-I00, funded by MCIN/AEI/10.13039/501100011033), the Comunidad de Madrid (IND2018/BMD-9804, MINA-CM-S2022/

BMD-7236, IND2023/BMD-28865, PIPF-2022_SAL-GL-2512, and PEJ-2019-AI/SAL-12703), the European Union's EIC-Pathfinder Program under the projects THOR (grant agreement number 101099719) and ISOS (grant agreement number 101130454), and funded by the Instituto de Salud Carlos III and cofunded by the European Regional Development Fund (FEDER) (project RD21/0006/0019).

REFERENCES

(1) Han, X.; Alu, A.; Liu, H.; Shi, Y.; Wei, X.; Cai, L.; Wei, Y. Biomaterial-assisted biotherapy: A brief review of biomaterials used in drug delivery, vaccine development, gene therapy, and stem cell therapy. *Bioact. Mater.* **2022**, *17*, 29−48.

(2) Tu, Z.; Zhong, Y.; Hu, H.; Shao, D.; Haag, R.; Schirner, M.; Lee, J.; Sullenger, B.; Leong, K. W. Design of therapeutic biomaterials to control inflammation. *Nat. Rev. Mater.* **2022**, *7* (7), 557−574.

(3) Kim, D.; Yoo, J. M.; Hwang, H.; Lee, J.; Lee, S. H.; Yun, S. P.; Park, M. J.; Lee, M.; Choi, S.; Kwon, S. H.; Lee, S.; Kwon, S.-H.; Kim, S.; Park, Y. J.; Kinoshita, M.; Lee, Y.-H.; Shin, S.; Paik, S. R.; Lee, S. J.; Lee, S.; Hong, B. H.; Ko, H. S. Graphene quantum dots prevent α-synucleinopathy in Parkinson's disease. *Nat. Nanotechnol.* **2018**, *13* (9), 812−818.

(4) (a) Mariner, P. D.; Wudel, J. M.; Miller, D. E.; Genova, E. E.; Streubel, S. O.; Anseth, K. S. Synthetic hydrogel scaffold is an effective vehicle for delivery of INFUSE (rhBMP2) to critical-sized calvaria bone defects in rats. *J. Orthop. Res.* **2013**, *31* (3), 401−406. (b) Silverman, J. A.; Deitcher, S. R. Marqibo(R) (vincristine sulfate liposome injection) improves the pharmacokinetics and pharmacodynamics of vincristine. *Cancer Chemother. Pharmacol.* **2013**, *71* (3), 555−564. (c) Ur Rehman, S. S.; Lim, K.; Wang-Gillam, A. Nanoliposomal irinotecan plus fluorouracil and folinic acid: a new treatment option in metastatic pancreatic cancer. *Expert Rev. Anticancer Ther.* **2016**, *16* (5), 485−492.

(5) Attenello, F. J.; Mukherjee, D.; Datoo, G.; McGirt, M. J.; Bohan, E.; Weingart, J. D.; Olivi, A.; Quinones-Hinojosa, A.; Brem, H. Use of Gliadel (BCNU) wafer in the surgical treatment of malignant glioma: a 10-year institutional experience. *Ann. Surg. Oncol.* **2008**, *15* (10), 2887−2893.

(6) (a) Samal, J.; Segura, T. Injectable biomaterial shuttles for cell therapy in stroke. *Brain Res. Bull.* **2021**, *176*, 25−42. (b) Zhang, Y.; Zou, Z.; Liu, S.; Miao, S.; Liu, H. Nanogels as Novel Nanocarrier Systems for Efficient Delivery of CNS Therapeutics. *Front. Bioeng. Biotechnol.* **2022**, *10*, 954470.

(7) Wang, Y.; Irvine, D. J. Engineering chemoattractant gradients using chemokine-releasing polysaccharide microspheres. *Biomaterials* **2011**, *32* (21), 4903−4913.

(8) Ju, R.; Wen, Y.; Gou, R.; Wang, Y.; Xu, Q. The experimental therapy on brain ischemia by improvement of local angiogenesis with tissue engineering in the mouse. *Cell Transplant.* **2014**, *23*, S83−S95.

(9) (a) Guziewicz, N. A.; Massetti, A. J.; Perez-Ramirez, B. J.; Kaplan, D. L. Mechanisms of monoclonal antibody stabilization and release from silk biomaterials. *Biomaterials* **2013**, *34* (31), 7766−7775. (b) Herdiana, Y.; Wathoni, N.; Shamsuddin, S.; Muchtaridi, M. Drug release study of the chitosan-based nanoparticles. *Heliyon* **2022**, *8* (1), No. e08674. (c) Yavuz, B.; Chambre, L.; Kaplan, D. L. Extended release formulations using silk proteins for controlled delivery of therapeutics. *Expert Opin. Drug Delivery* **2019**, *16* (7), 741−756.

(10) Yonesi, M.; Ramos, M.; Ramirez-Castillejo, C.; Fernandez-Serra, R.; Panetsos, F.; Belarra, A.; Chevalier, M.; Rojo, F. J.; Perez-Rigueiro, J.; Guinea, G. V.; Gonzalez-Nieto, D. Resistance to Degradation of Silk Fibroin Hydrogels Exposed to Neuroinflammatory Environments. *Polymers* **2023**, *15* (11), 2491.

(11) Tanna, V.; Sawarkar, S. P.; Ravikumar, P. Exploring Nose to Brain Nano Delivery for Effective Management of Migraine. *Curr. Drug Delivery* **2023**, *20* (2), 144−157.

(12) Flor, R. d. l.; Robertson, J.; Shevchenko, R. V.; Alavijeh, M.; Bickerton, S.; Fahmy, T.; Metcalfe, S. M. Multiple Sclerosis: LIFNano-CD4 for Trojan Horse Delivery of the Neuro-Protective Biologic "LIF" Into the Brain: Preclinical Proof of Concept. *Front. Med. Technol.* **2021**, *3*, 640569.

(13) Belda Marin, C.; Fitzpatrick, V.; Kaplan, D. L.; Landoulsi, J.; Guenin, E.; Egles, C. Silk Polymers and Nanoparticles: A Powerful Combination for the Design of Versatile Biomaterials. *Front. Chem.* **2020**, *8*, 604398.

(14) (a) Chen, M.; Shao, Z.; Chen, X. Paclitaxel-loaded silk fibroin nanospheres. *J. Biomed. Mater. Res., Part A* **2012**, *100A* (1), 203−210. (b) Pritchard, E. M.; Valentin, T.; Panilaitis, B.; Omenetto, F.; Kaplan, D. L. Antibiotic-Releasing Silk Biomaterials for Infection Prevention and Treatment. *Adv. Funct. Mater.* **2013**, *23* (7), 854−861.

(15) (a) Guziewicz, N.; Best, A.; Perez-Ramirez, B.; Kaplan, D. L. Lyophilized silk fibroin hydrogels for the sustained local delivery of therapeutic monoclonal antibodies. *Biomaterials* **2011**, *32* (10), 2642−2650. (b) Numata, K.; Reagan, M. R.; Goldstein, R. H.; Rosenblatt, M.; Kaplan, D. L. Spider silk-based gene carriers for tumor cell-specific delivery. *Bioconjugate Chem.* **2011**, *22* (8), 1605−1610.

(16) Wang, J.; Li, X.; Song, Y.; Su, Q.; Xiaohalati, X.; Yang, W.; Xu, L.; Cai, B.; Wang, G.; Wang, Z.; Wang, L. Injectable silk sericin scaffolds with programmable shape-memory property and neuro-differentiation-promoting activity for individualized brain repair of severe ischemic stroke. *Bioact. Mater.* **2021**, *6* (7), 1988−1999.

(17) Rahmatabadi, D.; Soltanmohammadi, K.; Aberoumand, M.; Soleyman, E.; Ghasemi, I.; Baniassadi, M.; Abrinia, K.; Bodaghi, M.; Baghani, M. 4D printing of porous PLA-TPU structures: effect of applied deformation, loading mode and infill pattern on the shape memory performance. *Phys. Scr.* **2024**, *99* (2), 025013.

(18) Atterberry, P. N.; Roark, T. J.; Severt, S. Y.; Schiller, M. L.; Antos, J. M.; Murphy, A. R. Sustained Delivery of Chemokine CXCL12 from Chemically Modified Silk Hydrogels. *Biomacromolecules* **2015**, *16* (5), 1582−1589.

(19) Lovett, M. L.; Wang, X.; Yucel, T.; York, L.; Keirstead, M.; Haggerty, L.; Kaplan, D. L. Silk hydrogels for sustained ocular delivery of anti-vascular endothelial growth factor (anti-VEGF) therapeutics. *Eur. J. Pharm. Biopharm.* **2015**, *95* (Pt B), 271−278.

(20) Wu, H.; Liu, S.; Xiao, L.; Dong, X.; Lu, Q.; Kaplan, D. L. Injectable and pH-Responsive Silk Nanofiber Hydrogels for Sustained Anticancer Drug Delivery. *ACS Appl. Mater. Interfaces* **2016**, *8* (27), 17118−17126.

(21) Fernandez-Garcia, L.; Mari-Buye, N.; Barios, J. A.; Madurga, R.; Elices, M.; Perez-Rigueiro, J.; Ramos, M.; Guinea, G. V.; Gonzalez-Nieto, D. Safety and tolerability of silk fibroin hydrogels implanted into the mouse brain. *Acta Biomater.* **2016**, *45*, 262−275.

(22) (a) Aznar-Cervantes, S. D.; Cenis, J. L.; Lozano-Picazo, P.; Bruno, A. L.; Pagan, A.; Ruiz-Leon, Y.; Candel, M. J.; Gonzalez-Nieto, D.; Rojo, F. J.; Elices, M.; Guinea, G. V.; Perez-Rigueiro, J. Unexpected high toughness of Samia cynthia ricini silk gut. *Soft Matter* **2022**, *18* (26), 4973−4982. (b) Madurga, R.; Ganan-Calvo, A. M.; Plaza, G. R.; Guinea, G. V.; Elices, M.; Perez-Rigueiro, J. Production of High Performance Bioinspired Silk Fibers by Straining Flow Spinning. *Biomacromolecules* **2017**, *18* (4), 1127−1133.

(23) Ritger, P. L.; Peppas, N. A. A simple equation for description of solute release II. Fickian and anomalous release from swellable devices. *J. Controlled Release* **1987**, *5* (1), 37−42.

(24) Peppas, N. A.; Sahlin, J. J. A simple equation for the description of solute release. III. Coupling of diffusion and relaxation. *Int. J. Pharm.* **1989**, *57* (2), 169−172.

(25) Sathe, P. M.; Tsong, Y.; Shah, V. P. In-vitro dissolution profile comparison: statistics and analysis, model dependent approach. *Pharm. Res.* **1996**, *13* (12), 1799−1803.

(26) (a) Ayuso, M. I.; Chioua, M.; Martinez-Alonso, E.; Soriano, E.; Montaner, J.; Masjuan, J.; Hadjipavlou-Litina, D. J.; Marco-Contelles, J.; Alcazar, A. CholesteroNitrones for Stroke. *J. Med. Chem.* **2015**, *58* (16), 6704−6709. (b) Martinez-Alonso, E.; Escobar-Peso, A.; Ayuso, M. I.; Gonzalo-Gobernado, R.; Chioua, M.; Montoya, J. J.; Montaner, J.; Fernandez, I.; Marco-Contelles, J.; Alcazar, A. Characterization of a CholesteroNitrone (ISQ-201), a Novel Drug Candidate for the Treatment of Ischemic Stroke. *Antioxidants* **2020**, *9* (4), 291.

https://doi.org/10.1021/acs.biomac.4c00629
Biomacromolecules 2024, 25, 5233−5250

(27) Blanco, V.; Camelo, J. L.; Carri, N. G. Growth inhibition, morphological differentiation and stimulation of survival in neuronal cell type (Neuro-2a) treated with trophic molecules. *Cell Biol. Int.* **2001**, *25* (9), 909−917.
(28) Machado, C. F.; Beraldo, F. H.; Santos, T. G.; Bourgeon, D.; Landemberger, M. C.; Roffe, M.; Martins, V. R. Disease-associated mutations in the prion protein impair laminin-induced process outgrowth and survival. *J. Biol. Chem.* **2012**, *287* (52), 43777−43788.
(29) DeCicco-Skinner, K. L.; Henry, G. H.; Cataisson, C.; Tabib, T.; Gwilliam, J. C.; Watson, N. J.; Bullwinkle, E. M.; Falkenburg, L.; O'Neill, R. C.; Morin, A.; Wiest, J. S. Endothelial cell tube formation assay for the in vitro study of angiogenesis. *J. Visualized Exp.* **2014**, *91*, No. e51312.
(30) Cancelas, J. A. Adhesion, migration, and homing of murine hematopoietic stem cells and progenitors. *Methods Mol. Biol.* **2011**, *750*, 187−196.
(31) Alonso, J. M.; Escobar-Peso, A.; Fernandez, I.; Alcazar, A.; Marco-Contelles, J. Improving the Efficacy of Quinolylnitrones for Ischemic Stroke Therapy, QN4 and QN15 as New Neuroprotective Agents after Oxygen-Glucose Deprivation/Reoxygenation-Induced Neuronal Injury. *Pharmaceuticals* **2022**, *15* (11), 1363.
(32) Mitra, K.; Chadha, A.; Muthuvijayan, V.; Doble, M. Self-Assembled Inhalable Immunomodulatory Silk Fibroin Nanocarriers for Enhanced Drug Loading and Intracellular Antibacterial Activity. *ACS Biomater. Sci. Eng.* **2022**, *8* (2), 708−721.
(33) Tomoda, B. T.; Pacheco, M. S.; Abranches, Y. B.; Vigano, J.; Perrechil, F.; De Moraes, M. A. Assessing the Influence of Dyes Physico-Chemical Properties on Incorporation and Release Kinetics in Silk Fibroin Matrices. *Polymers* **2021**, *13* (5), 798.
(34) Martin-Martin, Y.; Fernandez-Garcia, L.; Sanchez-Rebato, M. H.; Mari-Buye, N.; Rojo, F. J.; Perez-Rigueiro, J.; Ramos, M.; Guinea, G. V.; Panetsos, F.; Gonzalez-Nieto, D. Evaluation of Neurosecretome from Mesenchymal Stem Cells Encapsulated in Silk Fibroin Hydrogels. *Sci. Rep.* **2019**, *9* (1), 8801.
(35) Fernandez-Serra, R.; Martinez-Alonso, E.; Alcazar, A.; Chioua, M.; Marco-Contelles, J.; Martinez-Murillo, R.; Ramos, M.; Guinea, G. V.; Gonzalez-Nieto, D. Postischemic Neuroprotection of Amino-ethoxydiphenyl Borate Associates Shortening of Peri-Infarct Depolarizations. *Int. J. Mol. Sci.* **2022**, *23* (13), 7449.
(36) Koh, L.-D.; Cheng, Y.; Teng, C.-P.; Khin, Y.-W.; Loh, X.-J.; Tee, S.-Y.; Low, M.; Ye, E.; Yu, H.-D.; Zhang, Y.-W.; et al. Structures, mechanical properties and applications of silk fibroin materials. *Prog. Polym. Sci.* **2015**, *46*, 86−110.
(37) Young, S. A.; Riahinezhad, H.; Amsden, B. G. In situ-forming, mechanically resilient hydrogels for cell delivery. *J. Mater. Chem. B* **2019**, *7* (38), 5742−5761.
(38) Gharehnazifam, Z.; Dolatabadi, R.; Baniassadi, M.; Shahsavari, H.; Kajbafzadeh, A. M.; Abrinia, K.; Baghani, M. Computational analysis of vincristine loaded silk fibroin hydrogel for sustained drug delivery applications: Multiphysics modeling and experiments. *Int. J. Pharm.* **2021**, *609*, 121184.
(39) (a) Baggi, R. B.; Babu, K. N. Calculation of predominant drug release mechanism using Peppas-Sahlin model, Part-I (substitution method): A linear regression approach. *Asian J. Pharm. Technol.* **2016**, *6* (4), 128−137. (4) (b) Ghosal, K.; Chandra, A.; Rajabalaya, R.; Chakraborty, S.; Nanda, A. Mathematical modeling of drug release profiles for modified hydrophobic HPMC based gels. *Pharmazie* **2012**, *67*, 147−155.
(40) Orefice, L. L.; Waterhouse, E. G.; Partridge, J. G.; Lalchandani, R. R.; Vicini, S.; Xu, B. Distinct roles for somatically and dendritically synthesized brain-derived neurotrophic factor in morphogenesis of dendritic spines. *J. Neurosci.* **2013**, *33* (28), 11618−11632.
(41) Greenberg, D. A.; Jin, K. Vascular endothelial growth factors (VEGFs) and stroke. *Cell. Mol. Life Sci.* **2013**, *70* (10), 1753−1761.
(42) Cao, B. B.; Zhang, X. X.; Du, C. Y.; Liu, Z.; Qiu, Y. H.; Peng, Y. P. TGF-β1 Provides Neuroprotection via Inhibition of Microglial Activation in 3-Acetylpyridine-Induced Cerebellar Ataxia Model Rats. *Front. Neurosci.* **2020**, *14*, 187.
(43) (a) Cambier, S.; Gouwy, M.; Proost, P. The chemokines CXCL8 and CXCL12: molecular and functional properties, role in disease and efforts towards pharmacological intervention. *Cell. Mol. Immunol.* **2023**, *20* (3), 217−251. (b) Wang, Y.; Huang, J.; Li, Y.; Yang, G. Y. Roles of chemokine CXCL12 and its receptors in ischemic stroke. *Curr. Drug Targets* **2012**, *13* (2), 166−172.
(44) Zhang, Z. G.; Zhang, L.; Jiang, Q.; Zhang, R.; Davies, K.; Powers, C.; Bruggen, N.; Chopp, M. VEGF enhances angiogenesis and promotes blood-brain barrier leakage in the ischemic brain. *J. Clin. Invest.* **2000**, *106* (7), 829−838.
(45) Chi, E. Y.; Krishnan, S.; Randolph, T. W.; Carpenter, J. F. Physical stability of proteins in aqueous solution: mechanism and driving forces in nonnative protein aggregation. *Pharm. Res.* **2003**, *20* (9), 1325−1336.
(46) Li, A. B.; Kluge, J. A.; Guziewicz, N. A.; Omenetto, F. G.; Kaplan, D. L. Silk-based stabilization of biomacromolecules. *J. Controlled Release* **2015**, *219*, 416−430.
(47) Bini, E.; Knight, D. P.; Kaplan, D. L. Mapping domain structures in silks from insects and spiders related to protein assembly. *J. Mol. Biol.* **2004**, *335* (1), 27−40.
(48) (a) Candelario-Jalil, E.; Mhadu, N. H.; Al-Dalain, S. M.; Martínez, G.; Leon, O. S. Time course of oxidative damage in different brain regions following transient cerebral ischemia in gerbils. *Neurosci. Res.* **2001**, *41* (3), 233−241. (b) Lorenzano, S.; Rost, N. S.; Khan, M.; Li, H.; Batista, L. M.; Chutinet, A.; Green, R. E.; Thankachan, T. K.; Thornell, B.; Muzikansky, A.; Arai, K.; Som, A. T.; Pham, L. D.; Wu, O.; Harris, G. J.; Lo, E. H.; Blumberg, J. B.; Milbury, P. E.; Feske, S. K.; Furie, K. L. Early molecular oxidative stress biomarkers of ischemic penumbra in acute stroke. *Neurology* **2019**, *93* (13), e1288−e1298.
(49) Nih, L. R.; Gojgini, S.; Carmichael, S. T.; Segura, T. Dual-function injectable angiogenic biomaterial for the repair of brain tissue following stroke. *Nat. Mater.* **2018**, *17* (7), 642−651.
(50) Yanev, P.; van Tilborg, G. A.; van der Toorn, A.; Kong, X.; Stowe, A. M.; Dijkhuizen, R. M. Prolonged release of VEGF and Ang1 from intralesionally implanted hydrogel promotes perilesional vascularization and functional recovery after experimental ischemic stroke. *J. Cereb. Blood Flow Metab.* **2022**, *42* (6), 1033−1048.
(51) Cook, D. J.; Nguyen, C.; Chun, H. N. I.; L Llorente, I.; Chiu, A. S.; Machnicki, M.; Zarembinski, T. I.; Carmichael, S. T. Hydrogel-delivered brain-derived neurotrophic factor promotes tissue repair and recovery after stroke. *J. Cereb. Blood Flow Metab.* **2017**, *37* (3), 1030−1045.
(52) Agoston, D. V. How to Translate Time? The Temporal Aspect of Human and Rodent Biology. *Front. Neurol.* **2017**, *8*, 92.
(53) Hu, X.; Wang, Y.; Zhang, L.; Xu, M.; Zhang, J.; Dong, W. Magnetic field-driven drug release from modified iron oxide-integrated polysaccharide hydrogel. *Int. J. Biol. Macromol.* **2018**, *108*, 558−567.
(54) Haghighattalab, M.; Kajbafzadeh, A.; Baghani, M.; Gharehnazifam, Z.; Jobani, B. M.; Baniassadi, M. Silk Fibroin Hydrogel Reinforced With Magnetic Nanoparticles as an Intelligent Drug Delivery System for Sustained Drug Release. *Front. Bioeng. Biotechnol.* **2022**, *10*, 891166.
(55) Gharehnazifam, Z.; Dolatabadi, R.; Baniassadi, M.; Shahsavari, H.; Kajbafzadeh, A. M.; Abrinia, K.; Gharehnazifam, K.; Baghani, M. Multiphysics modeling and experiments on ultrasound-triggered drug delivery from silk fibroin hydrogel for Wilms tumor. *Int. J. Pharm.* **2022**, *621*, 121787.

https://doi.org/10.1021/acs.biomac.4c00629
Biomacromolecules 2024, 25, 5233−5250